Final assessment of superconducting (SC) and Pseudo Direct Drive (PDD) generator performance indicators (PI's).

Agreement n.:	308974
Duration	November 2012 – October 2017
Co-ordinator:	DTU Wind

The research leading to these results has received funding from the European Community's Seventh Framework Programme FP7-ENERGY-2012-1-2STAGE under grant agreement No. 308974 (INNWIND.EU).

Document information

Document Name:	Final assessment of SC and PDD PI's
Document Number:	Deliverable D 3.44
Author:	Asger Bech Abrahamsen, Dong Liu and Henk Polinder
Document Type	Report
Dissemination level	PU
Review:	Henk Polinder
Date:	27 October 2017
WP:	Electromechanical conversion WP3
Task:	Task 3.4
Approval:	Approved by WP Leader

TABLE OF CONTENTS

-

1 INTRODUCTION

The INNWIND.EU project has investigated innovative non-contact direct drive generator for the 10-20 MW turbine of the project. The focus has been on superconducting direct drive (SCDD) generators and magnetic pseudo direct drive (PDD) generators, because they can provide a torque density higher than what is possible with the current permanent magnet direct drive (PMDD) generators technology.

This report contains the final reporting on the properties of the generator designs obtained in the project and the comparison to reference drive trains.

The structure of the report is as following :

Chapter 2:	Superconducting direct drive generators
Chapter 3:	Magnetic pseudo direct drive generators
Chapter 4:	Reference drive train
Chapter 5:	Comparison of drive trains

1.1 Performance Indicators (PI) of the drive trains

The overarching PI of the drive trains is eventually the impact on Levelized Cost of Energy (LCoE) of the INNWIND.EU offshore turbine, when equipped with the specific drive trains. The LCoE is defined as

$$LCoE = \frac{\sum_{i=0}^{LT} C_i \frac{1}{(1+w)^i}}{\sum_{i=0}^{LT} E_i \frac{1}{(1+w)^i}} \qquad (1\text{-}1)$$

where C_i is the cost of commissioning, running and decommission in year i, LT is the life time, w is the interest rate of investing in the energy sector and E_i is the energy production of year i.

The following additional PI's are also defined

1.1.1 Size

The size of the generator is referring to the diameter D_{gen} and length L_{gen} of the radial flux direct drive electrical machines.

1.1.2 Weight

The weight of the generator m_{gen} contains both the active materials of the generator as well as the steel used to maintain a constant air gap on the generator.

1.1.3 Cost

The cost C_i is determined from the amount of active and structural materials in the generators and assumed unit mass costs.

1.1.4 Efficiency and Annual Energy production

The energy yield or annual energy production (AEP) of direct drive generators is determined from the assumed wind resource in the North sea.

1.1.5 Impact on LCoE

The levelized cost of energy can be evaluated in either absolute terms, if the cost of different technologies are well known, or in relative terms if the variation of some specific key performance indicators are known for different drive train.

2 SUPERCONDUCTING DIRECT DRIVE GENERATORS

2.1 Basic function

Superconducting direct drive generators can provide drive trains, which are compact and of low weight, but also expensive. If magnetic steel is added to the machines then expensive superconductor can be replaced by cheap steel, whereby the cost can be reduced but at the expense of a higher weight. It has been found in the INNWIND.EU project that the current properties of both the medium temperature MgB_2 superconductor and the high temperature $RBa_2Cu_3O_{6+x}$ coated conductor superconductor will require magnetic steel included in the machine in order to minimize the cost of the generator. The performance indicators of the INNWIND.EU superconducting generators are summarized in this section and will be compared in chapter 5.

2.2 MgB_2 superconducting direct drive generators

Magnesium di-boride MgB_2 is often referred to as a medium temperature superconductor due to the critical temperature of T_C = 39 K. It can be turned into wires by the Powder-In-Tube (PIT) process, where MgB_2 is drawn in tubes of Ni and made into a multifilament wires by combining many tubes and then rolling the final wires into a flat tape. A MgB_2 tape of 3.0 mm width and 0.7 mm thickness produced by Columbus superconductors has been investigated in the INNWIND.EU project.

2.2.1 Coil demonstration

A MgB_2 race track coil with an opening of 0.3 m and a straight section of 0.5 m has been tested to establish the superconducting properties of the MgB_2 tape as well as the cost being 4 €/m. Figure 2-1 is showing the race track coil consisting of 10 double pan cake coils, which were stacked into the race track coil. The cross section dimensions of the race track coil is 84 mm x 80 mm being similar to a field coil for a 10 MW direct drive generator. The coil holds about 5 km of MgB_2 tape.

The coil was ramped to a current of 145 A at T ~20 K and the voltage drop across the 10 double pan cake coils showed that 3 of them had a normal resistance in series with wire, which is indicating that the wire had been broken most likely during the winding. 8 of the coils showed short regions of weak superconductivity also indicating damage to the wire. 2 of the coils showed perfect superconducting properties.

The additional losses of the double pancake coil resulted in additional heating and a quench of the race track coil appeared. The soldering connection between 2 of the 10 coils burned out during the quench, but subsequent testing showed that most of the double pancake coil had the same properties after the quench.

It was concluded from the race track coil test that the MgB_2 tape was providing the expected superconducting properties, but that the winding process of the double pan cake coils is giving un-expected problems that will call for further work and industrialization. A wire qualification experiment was initiated after the coil test and will be reported in appendix A.

Based on the demonstration coil the technology readiness level of the coil is estimated to be TRL = 4 (Test in laboratory).

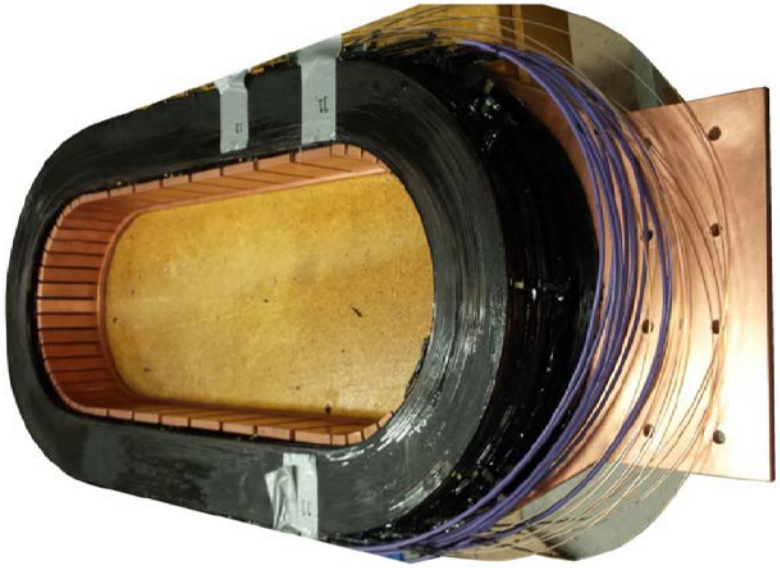

Figure 2-1 MgB_2 race track coil demonstration of the INNWIND.EU project. Reproduced from Deliverable report D3.13 (Magnusson, Hellesø, Paulsen, Eliassen, & Abrahamsen, 2016).

2.2.2 Topology optimization

A large effort has been made to determine a method for searching for the most optimal MgB_2 direct drive generator topology based on the Levelized Cost of Energy (LCoE) of the INNWIND.EU reference turbine and foundation. It has been found that iron cored generators are currently the most favorable designs, but that this might change if the following future developments of MbB_2 will be realized:

1) The unit cost of the MgB_2 tape is reduced to ¼ of the current cost (4 €/m -> 1 €/m)
2) The critical current density as function of applied magnetic field curve is increased be a factor of 4 for magnetic fields up to about 6 tesla.
3) Both scenario 1 and 2

In order to determine the properties of MgB_2 direct drive generators, the current cost and critical current density was used to design a 10 MW generator as shown in Figure 2-2. The design was then scaled to turbines with larger rotor diameters in order to determine the expected properties of a 20 MW generator.

The cost of the drive train was obtained from the material usage by applying the unit costs of Table 2-1, which are including manufacturing cost and profit. Thus these number are considerable higher than the raw materials cost.

Material	Unit cost
Copper (Cu)	15 €/kg
Glass fiber (G10)	15 €/kg
Steel laminates (Fe)	3 €/kg
Structural steel (Fe)	3-4 €/kg
MgB_2 (3.0 mm x 0.7 mm Columbus)	4 €/m

Table 2-1 Active material unit cost used in the MgB_2 generator design (Abrahamsen, Liu, & Polinder, 2017)

Table 2-2 and Table 2-3 are showing the mass and cost break down of the MgB_2 front mounted direct drive generator for the 10 MW and 20 MW version.

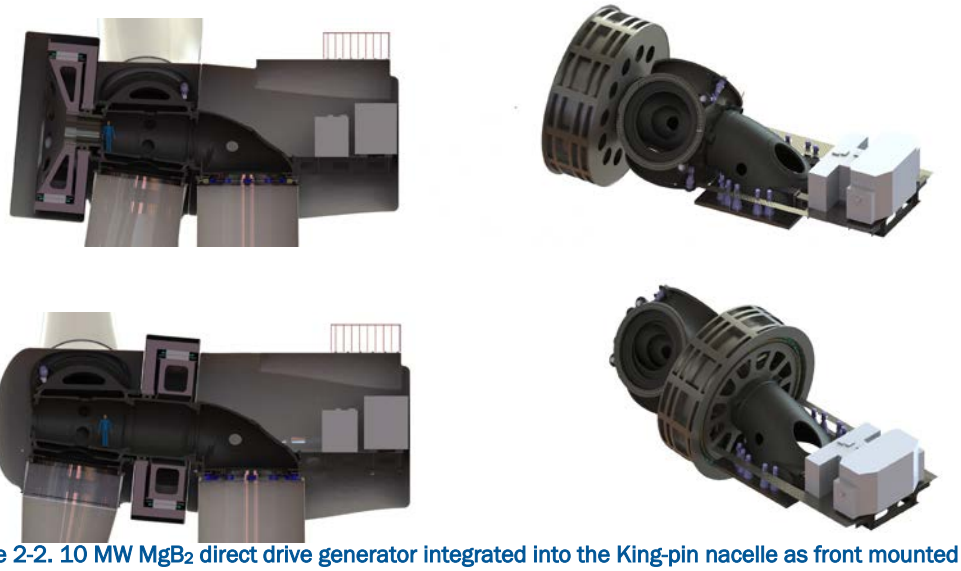

Figure 2-2. 10 MW MgB_2 direct drive generator integrated into the King-pin nacelle as front mounted (top) and in the downwind position (bottom). The diameter of the generator is D_{gen} = 8.4 m and the length L_{gen} = 1.3 m. The resulting weight of the front mounted generator is m_{gen} ~ 286 ton. Reproduced from Final Publication of INNWIND.EU and details can be found in deliverable report D3.41 (Stehouwer, van Zinderen, & Hossain, 2017).

Front mountedMgB$_2$ SCDD	D_{rotor}[m]	210	178	198	210	252	280
	CSF	Component mass [t]	Mass [t]	Mass [t]	Mass [t]	Mass [t]	Mass [t]
Hub	2,8	110	69,2	93,3	110,0	183,3	246,2
Blade	2,7	200	128,0	170,6	200,0	327,2	434,9
Pitch Bearings	2,5	28	18,5	24,2	28,0	44,2	57,5
Other Rotor parts	2,6	18	11,7	15,4	18,0	28,9	38,0
Main Bearings	3	5	3,0	4,2	5,0	8,6	11,9
Kingpin	2,8	50	31,5	42,4	50,0	83,3	111,9
Main shaft	2,8	0	0,0	0,0	0,0	0,0	0,0
Mainframe	2	73	52,4	64,9	73,0	105,1	129,8
Yaw bearing	2,3	9	6,2	7,9	9,0	13,7	17,4
Lantern	2	0	0,0	0,0	0,0	0,0	0,0
Main bearing housing	3	0	0,0	0,0	0,0	0,0	0,0
Other nacelle parts	2,5	35	23,2	30,2	35,0	55,2	71,8
Generator king-pin	2	13	9,3	11,6	13,0	18,7	23,1
Total nacelle		541	353,1	464,7	541,0	868,2	1142,5
Generator SCDD2	D_{rotor}[m]	178					
	CSF	Component mass [t]	Mass [t]	Mass [t]	Mass [t]	Mass [t]	Mass [t]
Active materials	2,17	118	118,0	148,7	168,9	250,9	315,4
Structural support	2,75	168	168,0	225,2	264,7	437,0	583,9
Total mass	2,75	286	286,0	373,8	433,6	687,9	899,3
RNA mass [t]			639,1	838,5	974,6	1556,2	2041,7
Rotor area [m^2]			24872	30775	34619	49851	61544
Turbine Power [MW] 400 W/m^2			9,9	12,3	13,8	19,9	24,6
Rotation speed [rpm]			9,6			7,13	
Rotation speed calculated [rpm]	0,85		9,6	8,8	8,3	7,1	6,5
Rotation speed [rad/sec]			1,00	0,92	0,87	0,75	0,68
Torque [MNm]			9,9	13,4	15,9	26,7	36,0

Table 2-2 Properties of MgB_2 front mounted direct drive generator shown in Figure 2-2 (top) when scaled for turbine rotor sizes between D = 178 m and to D = 280 m. The scaling is done by scaling per main component using the Cubic Scaling Factor (CSF), which is reduced below 3 for certain components, $m_2/m_1 = (D_2/D_1)^{CSF}$. Reproduced from table 9-4 of D3.11.

CFront mounted MgB_2 SCDD	10 MW	20 MW		10 MW	20 MW
	Mass [t]	Mass [t]	Mass cost [€/kg]	Cost [k€]	Cost [k€]
Hub	69,2	183,3	2,5	173	458
Blade	128,0	327,2	6,5	832	2130
Pitch Bearings	18,5	44,2	15,0	278	663
Other Rotor parts	11,7	28,9	2,5	29	72
Main Bearings	3,0	8,6	30,0	90	258
Kingpin	31,5	83,3	2,5	79	208
Main shaft	0,0	0,0	2,5	0	0
Mainframe	52,4	105,1	4,0	210	420
Yaw bearing	6,2	13,7	15,0	93	206
Lantern	0,0	0,0	4,0	0	0
Main bearing housing	0,0	0,0	4,0	0	0
Other nacelle parts	23,2	55,2	10,0	232	552
Generator king-pin	9,3	18,7	2,4	22	45
Total nacelle	353,1	868,2		2038	5012
Generator SCDD2					
Copper armature	13,1	24,3	15	197	365
Iron armature	49,4	106,7	3	148	320
MgB_2 rotor 4€/m	0,32	0,52	267	85	139
Iron rotor	51,8	111,5	3	155	335
Gen. Structural support	168	437	3	504	1311
Coldh & compres	1,8	4,7		223	563
Cryostats	3,4	8,9		377	951
Power converter	19,3	21,4		861	1595
Total	660	1583		4588	7558
Rotor area [m^2]	24872	49851			
Turbine Power [MW] 400 W/m^2	9,9	19,9			

Table 2-3 Mass and cost break down of components of the MgB_2 front mounted direct drive generator, Reproduced from table 9-5 of D3.11.

The partial loads losses of the MgB_2 drive train for 10 and 20 MW are shown in Figure 2-3 and Figure 2-4, which can be used to calculate the efficiency of the drive trains and then calculate the annual energy production by integrating the product of the mechanical power curve, the efficiency as function of wind speed and the wind speed distribution given by the Weibull distribution. The wind speed distribution is assumed to be characterized as a EIC class Ia, which has a mean wind speed of v_{ave} = 10.0 m/s and a shape parameter of k = 2. The integration is only taking the partial

load losses in to account from the cut-in wind speed and up to the rated wind speed, since the blade can be pitched slightly different above rated wind speed in order to compensate for the losses.

The analysis of the cooling system needed for the INNWIND.EU MgB_2 generators showed that the mapping of the SUPRApower cryostat and cooling system concept into the INNWIND.EU generators resulting in a power consumption for the cooling being about twice as much as shown in Figure 2-3 and Figure 2-4. Thus the efficiency curves used of the AEP integration includes 100 kW and 263 kW constant power consumption for the cooling.

The annual energy production (AEP) is reported below and is also compared to the ideal Annual Energy Production (AEP_0) given by assuming a loss free drive train. In that way one can calculate the fraction of the AEP to the ideal, which can be compared to any other drive trains.

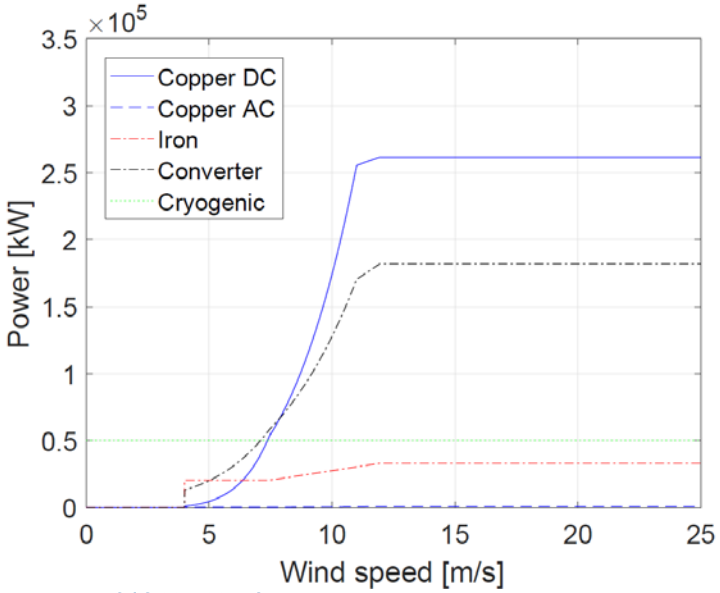

Figure 2-3 Partial load losses of 10 MW MgB2 direct drive generator. The cryogenic cooling power consumption is assumed to be 50 kW constantly (0.5 % of rated power).

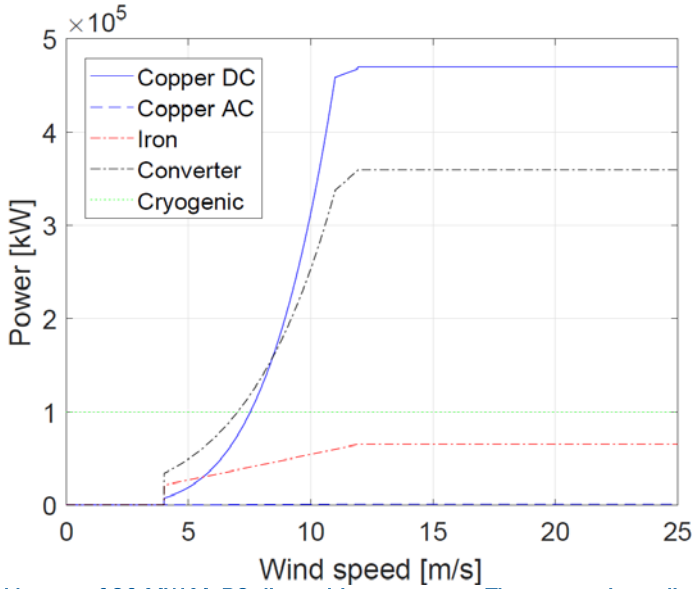

Figure 2-4 Partial load losses of 20 MW MgB2 direct drive generator. The cryogenic cooling power consumption is assumed to be 100 kW constantly (0.5 % of rated power).

2.2.3 Size

10 MW	D_{gen} = 8.4 m	L_{gen} = 1.3 m
20 MW	D_{gen} = 10.8 m	L_{gen} = 2.3 m

2.2.4 Weight

10 MW	$m_{gen,active}$ ~ 118 ton	$m_{gen,total}$ ~ 286 ton
20 MW	$m_{gen,active}$ ~ 251 ton	$m_{gen,total}$ ~ 688 ton

2.2.5 Cost

10 MW	$C_{gen,active}$ ~ 1.2 M€	$C_{gen,total}$ ~ 1.7 M€
20 MW	$C_{gen,active}$ ~ 2.7 M€	$C_{gen,total}$ ~ 4.0 M€

2.2.6 AEP and efficiency

10 MW	AEP =	48.3 GWh/year	AEP_0 =	49.8 GWh/year
20 MW	AEP =	95.7 GWh/year	AEP_0 =	99.0 GWh/year

2.2.7 LCoE

10 MW	$\Delta LCoE/ LCoE_0$ = 0.5 %
20 MW	$\Delta LCoE/ LCoE_0$ = 0.6 %

2.3 High temperature superconducting direct drive generators

The coated conductor high temperature superconductor is based on the compound $RBa_2Cu_3O_{6+x}$ (R = Rare Earth or Y), which has a critical temperature of T_C ~ 93 K for most of the rare earth elements. Coated conductors are made by depositing a 1 µm thin film of $RBa_2Cu_3O_{6+x}$ onto a steel or Hasteloy strip, whereby an almost single crystalline film of 12 mm width, 1 km length and 1 µm thickness is obtained. The critical current density of the film can reach 40000 A/mm^2 at T = 77 K and in the self field of the strip, but when including the thickness of the Hasteloy strip typical of 100 µm, then the effective critical current density is reduced to about 400 A/mm^2 at T = 77 K in self field. If the operation temperature is lowered toward T = 30 K then the critical current density is increased by a factor of 2-5 in magnetic flux densities of several tesla. The flat metal strip used in coated conductors has inspired to the name a tape instead of calling it a wire. Thus the high temperature superconductor is referred to as a coated conductor tape. The coated conductor tape is still made in relative small quantities and the cost used for the generator design is assumed to be 100 €/m for a 12 mm wide tape.

2.3.1 Coil demonstration

Siemens Wind Power has constructed and tested a race track field coil made from coated conductors in order to determine the properties of the material. The opening of the coil is 0.12 m and the length of the straight section is 0.3 m. The race track coil consist of 3 single layer coil staked on top of each other.
The coil was tested at T = 30 K using a liquid neon circuit and an operation current of I = 450 A was obtained before a damage was observed in the one of the coils. AC losses were measured before the increasing the current further towards the design current of 650 A. It was concluded that the coil and coated conductor would be able to meet the design specification, but further tests were not performed in order to measure the properties at the design point.

From the coated conductor race track coil manufacturing it was seen that several of the single layer coils were showing IV-curves, where weak superconductivity was measured. 5 coils out of 8 passed the test of the superconducting properties in liquid nitrogen (T = 77 K). 3 coils were selected for the race track construction at T = 30 K, but one of the coils also showed as partial damage. Thus the Technology Readiness Level of the coated conductor coil manufacturing must be concluded to be at TRL ~ 4 (tested in laboratory environment). Industrialization of the coil manufacturing is needed in order to raise the TRL level further.

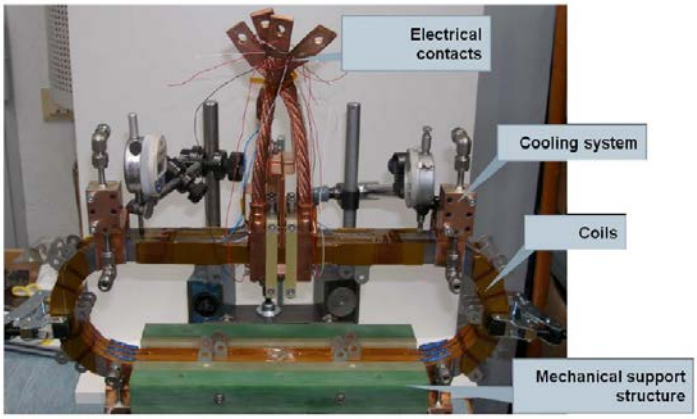

Figure 2-5 Coated conductor race track coil demonstrated by Siemens Wind Power. Reproduced from Fig 9 in D3.12 (Thomas & Azar, 2016).

2.3.2 Machine optimization

The coated conductor properties obtained from the race track coil has been used to optimize a 10 MW and 20 MW direct drive wind turbine generator. The topologies investigated were air cored as well as iron cored generator designs as shown in Figure 2-6. It was found that the iron cored generators were needed in order to reduce the usage of the coated conductor and thereby reduce the cost of the generator. The properties of the coated conductor direct drive generators are shown in Table 2-4 and Figure 2-7 is illustrating the pole structure.

Material	Unit cost
Copper (Cu)	7.5 €/kg
Steel laminates (Fe)	0.8 €/kg
Structural steel (Fe)	€/kg (Non investigated)
$RBa_2Cu_2O_{6+x}$ (12 mm wide coated conductor)	100 €/m

Table 2-4 Unit cost of active material used by Siemens Wind Power to optimize the coated conductor high temperature superconducting direct drive generators (Guan & et. al., 2017).

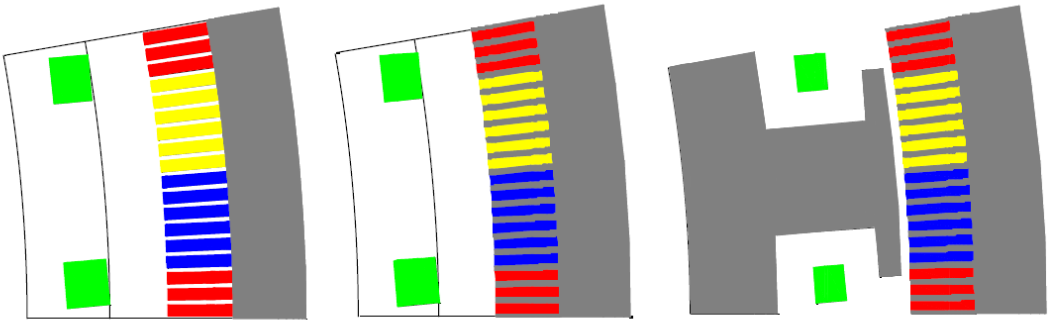

Figure 2-6 Topologies ranging from air cored to iron cored machines investigated for the coated conductor high temperature superconducting direct drive generators. The superconducting field winding is shown as a green box and the 3 phase armature windings are marked with red, yellow and blue respectively. Iron laminates are shown as grey. a) Air cored rotor and armature with non-magnetic teeth. b) Air cored rotor and magnetic teeth was added to the armature, c) Both iron cored field and armature windings. Reproduced from Fig 19 in D3.12 (Thomas & Azar, 2016).

	10MW	20MW-I	20MW-II
Stator outer diameter D (m)	7	7	11
Stack length L (m)	1.2	1.95	1.16
Speed n (rpm)	9.6	6.8	6.8
Torque T_{em} (MNm)	10.5	30	30
Stator current density J_s(A/mm2)	3.5	3.5	3.5
Stator slot packing factor	0.6	0.6	0.6
Number of poles 2p	32	32	64
Number of stator slots Q	384	384	768
Air gap length g (mm)	9	9	13
SC current density J_{SC} (A/mm2)	340	273	340
SC area per pole (mm2)	200	1000	200
Length of SC wire (km)	5.35	39.2	10.54
Ampere turns of SC per pole (AT)	34,000	136,500	34,000
Type of stator core	Iron-core	Iron-core	Iron-core
Type of rotor core	Iron-core	Iron-core	Iron-core
Volume of generator (m^3)	42.3	68.7	100.5
Mass of Iron (t)	141	271.9	208
Cost of SC (million €)	0.543	3.92	1.054
Cost of Cu (million €)	0.117	0.215	0.192
Cost of iron (million €)	0.112	0.217	0.166
Cost of total (million €)	0.764	4.35	1.412

Table 2-5 Properties of the coated conductor high temperature direct drive generators for 10 MW and 20 MW. Reproduced from Table 14 in D3.12 (Thomas & Azar, 2016).

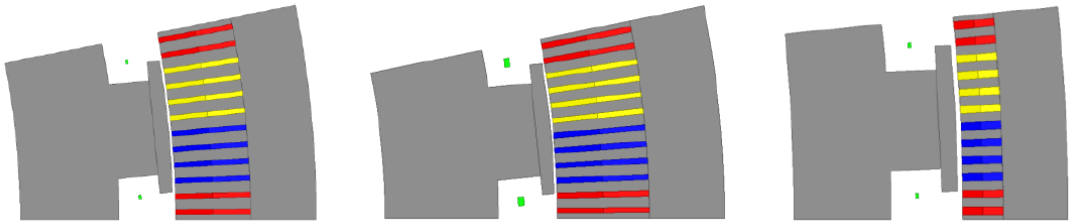

(a) 10MW, D=7m, 2p=32. (b) 20MW, D=7m, 2p=32. (c) 20MW, D=11m, 2p=64.

Figure 2-7 Illustration of the pole cross section of the coated conductor direct drive generators found in Table 2-4. A) the 10 MW generator with a diameter of 7 m and 32 poles. B) the 20 MW generator with a diameter of 7 m and 32 poles. C) 20 MW generator with a diameter of 11 m and 64 poles. Reproduced from Fig 80 in D3.12 (Thomas & Azar, 2016).

The partial load efficiency of the 10 MW coated conductor direct drive generator is show in Figure 2-8, where the power converter efficiency is also included. The power consumption of the cooling system is however not included in the plot, because the specification of the cooling system was not completed as Siemens Wind Power concluded that coated conductor technology is considerable more expensive that the Permanent Magnet Direct Drive.

The performance indicators of the coated conductor direct drive generators haven been calculated as reported in the sections below.

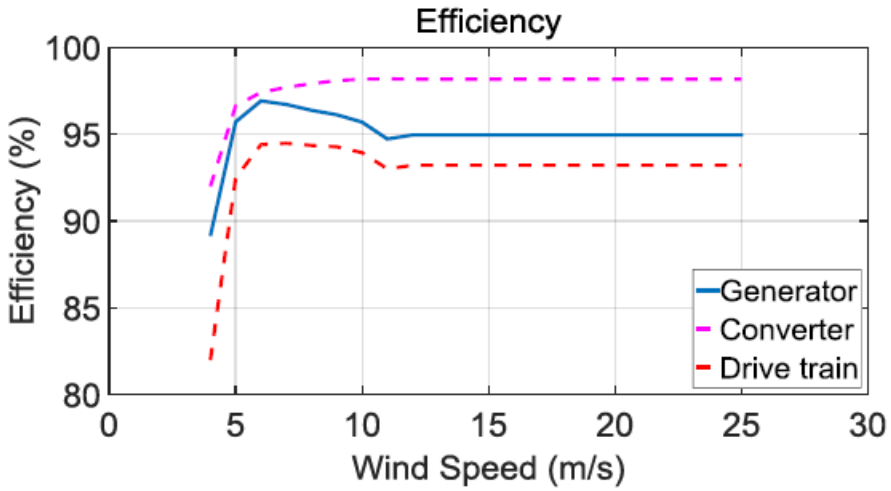

Figure 2-8 Partial load efficiency of 10 MW coated conductor direct drive generator (Reproduced from Fig 89 in D3.12 (Thomas & Azar, 2016)).

2.3.3 Size

10 MW	D_{gen} = 7.0 m	L_{gen} = 1.2 m
20 MW	D_{gen} = 11.0 m	L_{gen} = 1.2 m

2.3.4 Weight

10 MW	$m_{gen,active}$ ~ 156 ton
20 MW	$m_{gen,active}$ ~ 233 ton

2.3.5 Cost

10 MW	$C_{gen,active}$ ~ 0.76 M€
20 MW	$C_{gen,active}$ ~ 1.41 M€

2.3.6 AEP

10 MW	AEP = 48.5 GWh/year	AEP_0 = 49.8 GWh/year
20 MW	-	

2.3.7 LCoE

10 MW	$\Delta LCoE/ LCoE_0$ = -1.0 %
20 MW	-

3 MAGNETIC PSEUDO DIRECT DRIVE

3.1 Basic function

The PDD is a magnetic and mechanical integration of a magnetic gear system and a permanent magnet generator as illustrated in Figure 3-1. The inclusion of a single stage gear gives an uplift in performance to the generator system, i.e. increased rotor speed, reduced airgap torque and increased efficiency whilst allowing the size and mass of the generator to be minimized.

The magnetic gearbox converts high torque and slow rotation speed of the pole piece (PP) rotor (connected to the blades) into a faster rotation of an inner permanent magnet rotor. The magnetic field of the inner rotor interacts with the outer armature windings, where a higher voltage is induced due to the higher rotation speed. This allows a smaller current in the armature windings and thereby lower Joule heating due to the resistance of the copper windings. Thus the PDD can provide a compact drive train and at the same time an efficiency which is considerably higher than other wind turbine drive trains. Figure 3-1 shows the design of a PDD for a small wind turbine with a rated torque of 200 kNm and Figure 3-2 shows the integration of the PDD into the 10 MW INNWIND.EU reference turbine. Figure 3-3 shows detail of the king-pin and bearing arrangement of the front-mounted 20MW PDD.

The construction of the pole-piece rotor for large generators is a technical challenge, which has been investigated during the INNWIND.EU project. The 200 kNm PDD generator is constructed in a commercial project by Magnomatics at the end of the INNWIND.EU project. The outcomes of the project will be made available to the INNWIND.EU consortium following testing.

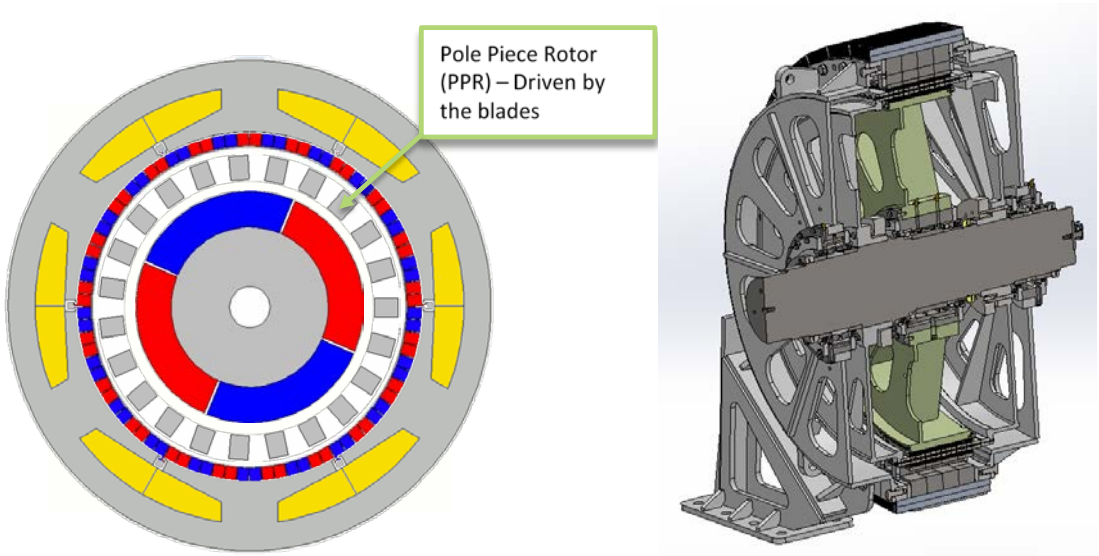

Figure 3-1 Left: Illustration of magnetic Pseudo direct drive generator. The inner rotor holds permanent magnets, which are rotating at around 7 times the speed of the pole-piece rotor consisting of a large number of laminated magnetic pole-pieces. The armature windings are mounted in the stationary outer generator structure. Right: Illustration of the PDD generator intended for a 200 kNm wind turbine that will be manufactured and tested by Magnomatics in Q2 2018. Reproduced from final publication of INNWIND.EU.

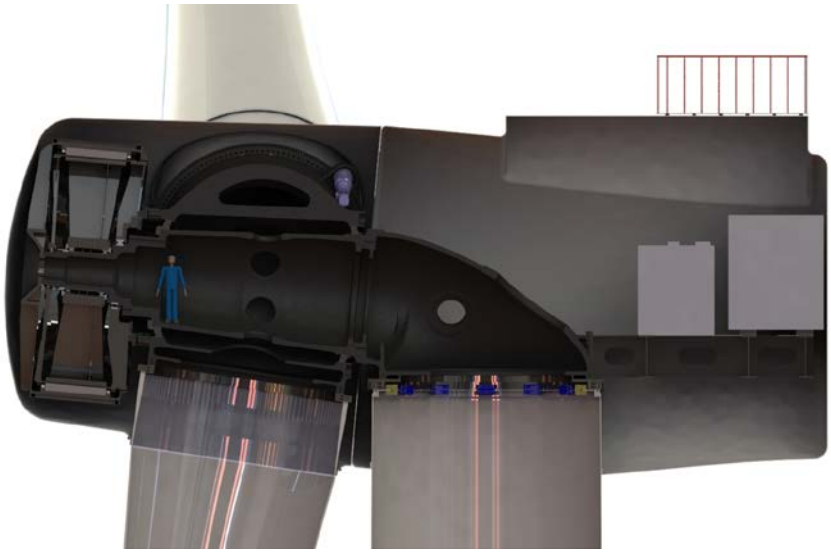

Figure 3-2 Magnetic Pseudo Direct Drive (PDD) generator mounted in front of the INNWIND.EU 10 MW turbine. The diameter of the generator is D_{gen} = 6.0 m and the length is L_{gen} = 1.66 m. The generator weight is estimated to be m_{gen} = 150 ton. Reproduced from Final publication of INNWIND.EU.

Figure 3-3 – 20MW Magnetic PDD generator that is designed for front-mounted operation. The torque-only coupling allows bearings to be sized based on the generators own static and dynamic loads. The king-pin type design reacts main torque through the central stub-shaft of the PDD.

3.2 Properties

The design parameters and performance specification of a PDD for 10MW and 20MW INNWIND.EU front mounted generators is outlined in Table 3-1. The assumed unit cost of the active materials are listed in Table 3-2.

Symbol	Quantity	Value for 10MW	Value for 20MW
	Rated power	10 MW	20MW
$\Omega_{PP,R}$	Rated speed of PP rotor	9.65 rpm	6.82 rpm
	Rated torque on the PP rotor	9.9 MNm	28.0 MNm
	Analytical pullout torque of the MG	11.9 MNm	33.7 MNm
$f_{out,R}$	Rated electrical output frequency	48.25 Hz	34.1 Hz
G	Gear ratio	7.5	7.5
p_{HS}^*	Pole-pairs on HS rotor per section	2	2
p_S^*	Pole-pairs on stator per section	13	13
m_S	Halbach segments per pole-pair on the stator	4	4
Q^*	Pole-pieces per section	15	15
S	Number of identical sections	20	20
	PP slot opening angle	$\pi/300$ rad	$\pi/300$ rad
D	Airgap diameter	6.0 m	8.5 m
w_{PP}	Radial thickness of PPs	31.4 mm	44.4 mm
	Radial thickness of HS rotor PMs	39.8 mm	56.3 mm
	Radial thickness of stator PMs	25.2 mm	35.6 mm
	Length of inner airgap	6.0 mm	8.5 mm
	Length of outer airgap	6.0 mm	8.5 mm
l_a	Active axial length	1.66 m	2.35 m
	HS rotor pole arc to pole pitch ratio	0.8	0.8
B_r	Remanence of N48SH PMs at 100°C	1.25 T	1.25 T
μ_r	Relative recoil permeability of PMs	1.05	1.05
	Copper packing factor	0.5	0.5
	Current density at rated power	2.0 A_{rms}/mm^2	2.0 A_{rms}/mm^2
	Annual energy efficiency	98.4%***	98.4%***
	PM mass	13.5 tons	38.2 tons
	HS rotor and PP rotor laminated steel mass	14 tons	39.6 tons
	Stator laminated steel mass	15.5 tons	74 tons
	Copper mass	7 tons	14 tons
	Estimated structural mass **	100 tons	254 tons
	Estimated total mass	150 tons	420 tons

Table 3-1 Properties of Magnetic Pseudo Direct Drive (PDD) generators for 10 MW and 20 MW INNWIND.EU turbines. Reproduced from Deliverable D3.21 (Penzkofer & Atallah, 2015) and updated with recent structural mass estimate**.

Material	Unit cost
Copper (Cu)	15 €/kg
Steel laminates (Fe)	3 €/kg
Structural steel (Fe)	3 €/kg
PM (B_{rm} = 1.25 T and μ_{rm} = 1.05)	58 €/kg

Table 3-2 Properties of active and structural materials of the magnetic Pseudo Direct drive (PDD) generator design. Reproduced from Table 2-1 and magnet price taken from the most up-to-date quotations received by Magnomatics for volume supply of fully processed, coated material.

The effect of the combination of the magnetic gearbox and the armature winding results in the efficiencies shown in Figure 3-4 Partial load efficiency of the magnetic Pseudo direct drive generator for 10 MW and 20 MW INNWIND.EU turbines. Reproduced from Fig 45 in D3.21 (Penzkofer & Atallah, 2015).

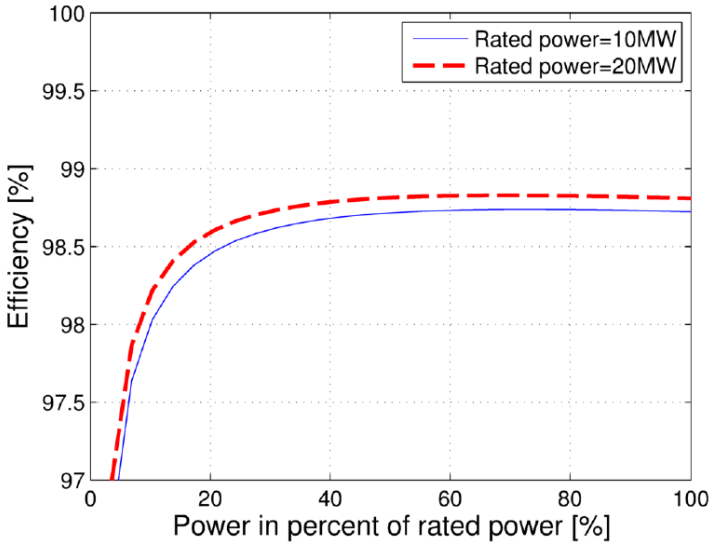

Figure 3-4 Partial load efficiency of the magnetic Pseudo direct drive generator for 10 MW and 20 MW INNWIND.EU turbines. Reproduced from Fig 45 in D3.21 (Penzkofer & Atallah, 2015).

A more rigorous treatment of the loss breakdown in large PDDs has been carried out by Magnomatics, including bearing losses, finite element analysis of magnet eddy currents and stray losses (eddy currents) in the structural components. The updated efficiency at rated load reduces from the 98.75% reported in the basic loss analysis of Atallah and Penzkofer (D3.21 and shown graphically in Figure 3-4) to 98.44% on consideration of these losses for the 20MW PDD. This still represents a significant efficiency (and thus LCOE) advantage over all other known competing technologies.

Table 3-3 shows the estimated breakdown of losses as a function of total loss at rated load in a 20MW PDD at the rated frequency of 34.1Hz. Previous efficiency estimates (D3.21 and shown graphically in Figure 3-4) only considered the copper and iron loss. The modelling techniques (some of which are unique to PDDs and magnetic gears) allow a more mature efficiency estimate to be made of the efficiency over a cubic load curve (see Figure 3-5).

Table 3-3 – Loss breakdown estimate as a percentage of total loss at rated power for a 20 MW PDD based on 200 kNm predictions and measured results from the 16 kNm machine.

Loss component	% of total loss at rated power [%]
Copper loss	45.7
PPR iron loss	7.4
Stator iron loss	22.1
Stator magnet loss	12.6
HSR magnet loss	6.3
PPR tie-rods	1.9
Compression plates	1.3
Mild steel endplates	1.3
Bearings (estimate)	1.6

Although it can be seen from Table 3-3 that the copper loss and iron loss still make up >75% of the total machine loss, the magnet eddy current loss makes up close to 19% of the total loss whilst the remaining structural material eddy current losses and bearing loss totals just over 6%. It has been reported in D1.25 that the magnet eddy current loss is a function of CAPEX, as the greater the segmentation applied to the magnets, the lower the loss will be, but the higher the costs.

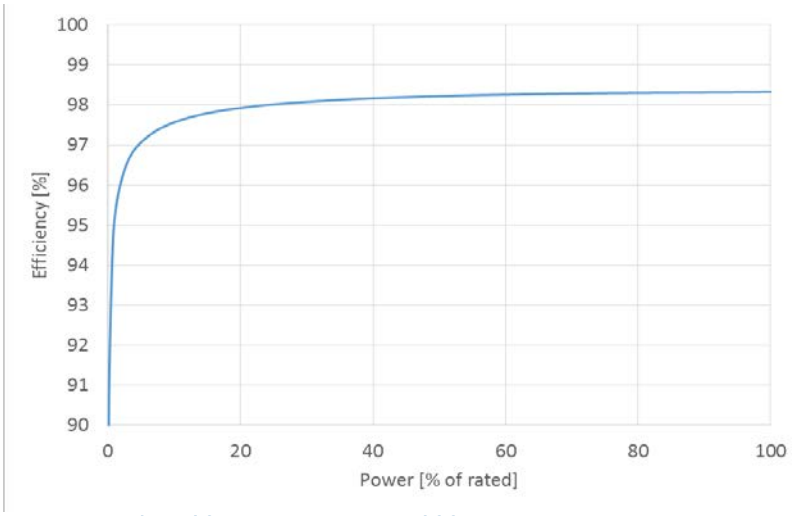

Figure 3-5 - Efficiency curve for a 20 MW PDD based on 200 kNm predictions and measured results from the 16 kNm machine.

3.2.1 Size

10 MW	D_{gen} = 6.0 m	L_{gen} = 1.7 m
20 MW	D_{gen} = 8.5 m	L_{gen} = 2.4 m

3.2.2 Weight

10 MW	$m_{gen,active}$ ~ 50 ton	$m_{gen,total}$ ~ 150 ton
20 MW	$m_{gen,active}$ ~ 166 ton	$m_{gen,total}$ ~ 420 ton

3.2.3 Cost

Cost breakdown for 10 MW and 20 MW PDD designs below consider a magnet price of €58/kg.

10 MW	$C_{gen,active}$ ~ 0.96 M€	$C_{gen,total}$ ~ 1.25 M€
20 MW	$C_{gen,active}$ ~ 2.7 M€	$C_{gen,total}$ ~ 3.5 M€

If the magnet price per kilogram is taken to be that of the reference design (€25/kg) then the costs will reduce significantly as shown below. However, it is recognized that the magnet processing (segmentation) required in large PDD generators will result in a higher relative cost per kilogram (possibly somewhere between these two sets of figures).

10 MW	$C_{gen,active}$ ~ 0.8 M€	$C_{gen,total}$ ~ 1.13 M€
20 MW	$C_{gen,active}$ ~ 1.5 M€	$C_{gen,total}$ ~ 2.3 M€

3.2.4 AEP and efficiency

10 MW	AEP =	49.2 GWh/year	AEP_0 =	49.8 GWh/year
20 MW	AEP =	97.6 GWh/year	AEP_0 =	99.0 GWh/year

3.2.5 LCoE

10 MW	$\Delta LCoE/ LCoE_0$ = -1.91 %
20 MW	$\Delta LCoE/ LCoE_0$ = -2.05 %

4 REFERENCE DRIVE TRAINS

4.1 Description

The reference drive trains are based on the 10 MW Direct-Drive PM generator presented by Polinder et al. (Polinder H. , 2007) The generator topology is shown in Figure 4-1 and is based on surface mounted $R_2Fe_{14}B$ permanent magnets. Table 4-1 is showing the unit cost of the active materials and it should be noted that the cost of the R-Fe-B permanent magnets has changed a lot during the INNWIND.EU project. At the beginning of the INNWIND.EU project there had just been a price bobble on the R-Fe-B permanent magnets and unit cost levels were quoted up to 150 €/kg. This cost has however been reduced considerable and it is believed that the level of 25 €/kg in the paper by Polinder from 2007 is about to be the same level as is seen from materials coming out of China today.

The PMDD reference generator is extended to include two designs – with a shear stress of 40 kN/m^2, and 60 kN/m^2. The use of the higher shear stress results in a machine with a lower rated efficiency, but an improved partial load efficiency.

Furthermore, a medium speed PM generator is also designed and represent the drive train of the INNWIND.EU reference turbines.

This gives a total of six designs, which are listed below:

- 10 MW PM Direct-Drive : Option I (shear stress = 40 kN/m^2).
- 10 MW PM Direct-Drive : Option II (shear stress = 60 kN/m^2).
- 10 MW Medium Speed PM.
- 20 MW PM Direct-Drive : Option I (shear stress = 40 kN/m^2).
- 20 MW PM Direct-Drive : Option II (shear stress = 60 kN/m^2).
- 20 MW Medium Speed PM.

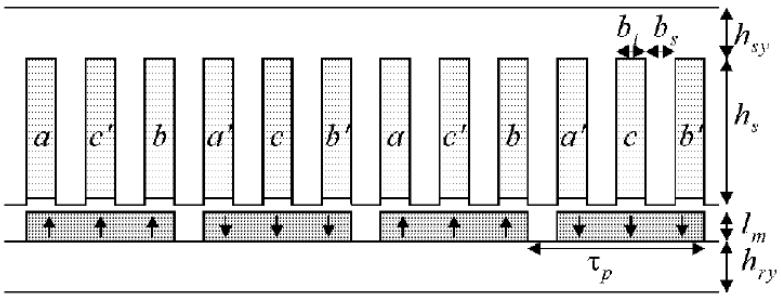

Figure 4-1 Illustration of the active materials of the Permanent magnet direct drive generator by Polinder, which is used as reference for the comparison of the INNWIND.EU drive trains. Reproduced from

4.2 Assumptions

Table 4-1 presents the assumptions used in the design of the reference generators.

	unit	Direct-Drive	Medium Speed
	Gearbox Characteristics		
Gear Ratio – 10 MW turbine		-	50
Gear Ratio – 20 MW turbine		-	48
Gearbox Mass Constant	kg/kNm	-	13.25
Gearbox Losses (modelled as const. Friction Torque)		-	1% per stage
	Generator Characteristics		
Slot fill factor		0.65	0.65
Magnet Remanent Flux Density (B_{rm})	T	1.2	1.2
Magnet Recoil Permeability		1.06	1.06
Resistivity of Copper (at 100°C)	Ωm	2.52E-8	2.52E-8
Eddy Current Losses in Lamination (P_{Fe0e})	W/kg	1	1
Hysteresis Losses in Lamination (P_{Fe0e})	W/kg	4	4
	Cost		
Laminations	€/kg	3	3
Copper	€/kg	15	15
PM	€/kg	25	25
Structural Steel	€/kg	3	3
Gearbox	€/kg	-	12

Table 4-1 Design assumption of active material properties and cost of the reference drive trains.

4.3 10 MW Reference Turbine

On the basis of the assumptions stated in the previous section, the generated designs are presented in the table below:

	unit	Direct-Drive		Medium Speed
		OPTION – I	OPTION – II	
Rated Speed	rpm	9.6	9.6	480
Pole Pairs		160	160	8
Rated Frequency	Hz	25.46	25.46	64.00
Shear Stress	kN/m²	~40	~60	~40
	Generator Dimensions			
Airgap Radius	m	5	5	0.80
Stack Length	m	1.68	1.12	1.36
Airgap Length	mm	10	10	7
Slot Height	mm	80	80	80
Stator Yoke Height	mm	40	40	140
Rotor Yoke Height	mm	40	40	140
Tooth Width to Tooth Pitch Ratio		0.5	0.5	0.55
Slots per Pole per Phase (q)		1	1	3
Magnet Length	mm	20	20	30
Magnet Width to Pole Ratio (α)		0.8	0.8	0.8
	Weights			
Laminations	ton	48.93	32.62	17.54
Copper	ton	13.64	9.57	2.08
PM	ton	6.40	4.27	0.82
Gearbox	ton	-	-	137.07

Table 4-2 Properties of 10 MW reference drive trains for INNWIND.EU comparison.

4.3.1 Direct-Drive Performance

The partial loads losses of the 10 MW Direct-Drive drive train for the two reference generators are shown in Figure 4-1 and Figure 4-2.

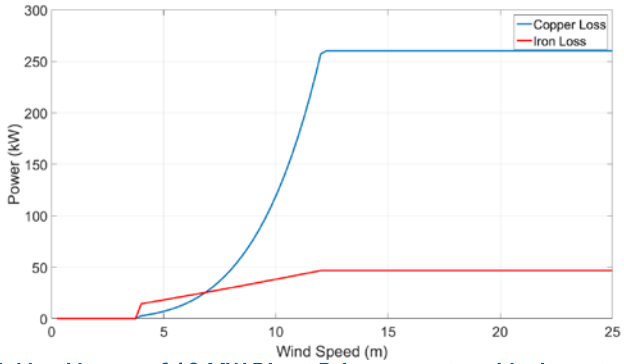

Figure 4-2 Partial load losses of 10 MW Direct-Drive generator with shear stress of 40 kN/m².

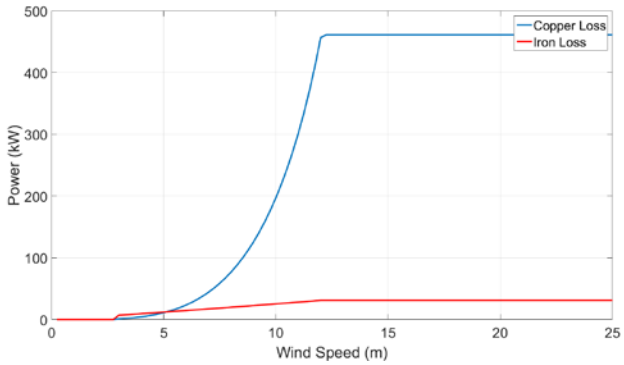

Figure 4-3 Partial load losses of 10 MW Direct-Drive generator with shear stress of 60 kN/m².

These losses result in efficiency curves as presented in Figure 4-3.

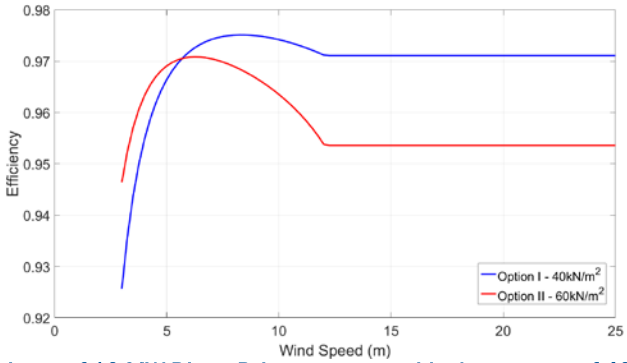

Figure 4-4 Efficiency of 10 MW Direct-Drive generator with shear stress of 40 and 60 kN/m².

4.3.1.1 Size

10 MW
Option I D_{gen} = 10 m L_{gen} = 1.68 m
Option II D_{gen} = 10 m L_{gen} = 1.12 m

4.3.1.2 Weight

10 MW
Option I $m_{gen,active}$ ~ 69 ton $m_{gen,total}$ ~ 237 ton
Option II $m_{gen,active}$ ~ 46.5 ton $m_{gen,total}$ ~ 214.5 ton

The weight of the support structure is assumed to be equal to that of the superconducting Direct-Drive generator.

4.3.1.3 Cost

10 MW
Option I $C_{gen,active}$ ~ 0.51 M€ $C_{gen,structure}$ ~ 0.50 M€ $C_{gen,total}$ ~ 1.01 M€
Option II $C_{gen,active}$ ~ 0.35 M€ $C_{gen,structure}$ ~ 0.50 M€ $C_{gen,total}$ ~ 0.85 M€

4.3.1.4 AEP and efficiency

10 MW
Option I AEP = 48.9 GWh/year AEP_0 = 49.8 GWh/year
Option II AEP = 48.7 GWh/year

4.3.1.5 LCoE

Option I $\Delta LCoE/ LCoE_0$ = -1.52 %
Option II $\Delta LCoE/ LCoE_0$ = -1.32 %

4.3.2 Medium Speed Drive train Performance

The partial loads losses of the 10 MW medium speed drive train is shown in Figure 4-4.

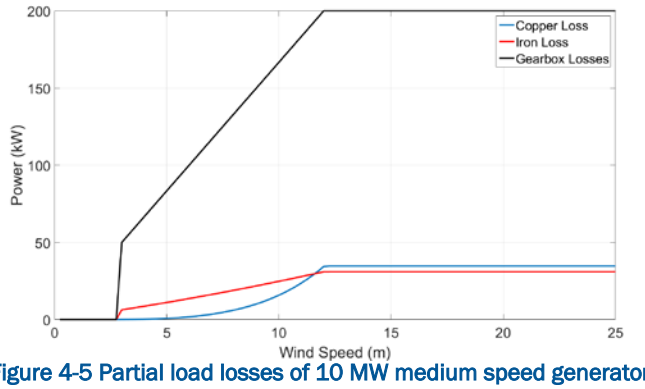

Figure 4-5 Partial load losses of 10 MW medium speed generator.

These losses result in efficiency curves as presented in Figure 4-5.

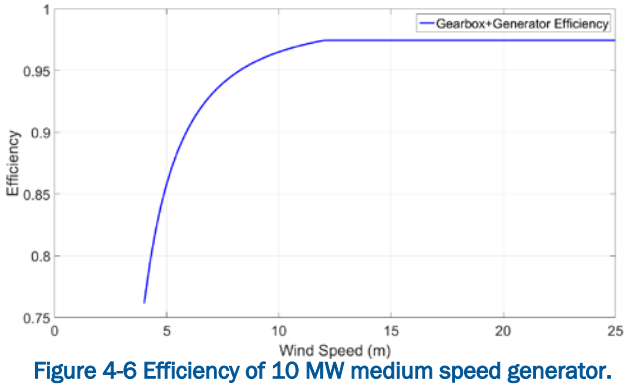

Figure 4-6 Efficiency of 10 MW medium speed generator.

4.3.2.1 Size

10 MW	D_{gen} = 1.6 m	L_{gen} = 1.36 m

4.3.2.2 Weight

10 MW	$m_{gen,active}$ ~ 20.5 ton M_{gear} ~ 137.1 ton	$m_{gen,total}$ ~ 41 ton $m_{drive,total}$ ~ 178 ton

The weight of the support structure is assumed to be equal to that medium speed generator (Polinder, Van der Pijl, De Vilder, & Tavner, 2006) .

4.3.2.3 Cost

10 MW	$C_{gen,active}$ ~	0.13 M€	$C_{gearbox}$ ~	1.65 M€
	$C_{gen,structure}$ ~	0.06 M€	C_{total} ~	1.84 M€

4.3.2.4 AEP and efficiency

10 MW	AEP =	48.5 GWh/year	AEP_0 =	49.8 GWh/year

4.3.2.5 LCoE

10 MW	$\Delta LCoE / LCoE_0$ = 0 %	(Used as reference drive train for LCoE)

4.4 20 MW Reference Turbine

The designs for the 10 MW drivetrains is scaled to generate designs for a 20 MW drivetrain. The details of the design are given in Table 4-3 below:

	unit	Direct-Drive		Medium Speed
		OPTION – I	OPTION – II	
Rated Speed	rpm	7.13	7.13	342.24
Pole Pairs		220	220	10
Rated Frequency	Hz	26.15	26.15	57.04
Shear Stress	kN/m^2	~40	~60	~40
	Generator Dimensions			
Airgap Radius	m	7	7	1.1
Stack Length	m	2.25	1.5	1.9
Airgap Length	mm	14	14	8.5
Slot Height	mm	80	80	80
Stator Yoke Height	mm	40	40	150
Rotor Yoke Height	mm	40	40	150
Tooth Width to Tooth Pitch Ratio		0.5	0.5	0.55
Slots per Pole per Phase (q)		1	1	3
Magnet Length	mm	30	30	30
Magnet Width to Pole Ratio (α)		0.8	0.8	0.8
	Weights			
Laminations	ton	91.60	61.06	35.36
Copper	ton	24.93	17.30	3.73
PM	ton	18.01	12.01	2.38
Gearbox	ton	-	-	362.02

Table 4-3 Properties of 20 MW reference drive train.

4.4.1 Direct-Drive Performance

The partial loads losses of the 20 MW Direct-Drive drive train for the two reference generators are shown in Figure 4-6 and Figure 4-7.

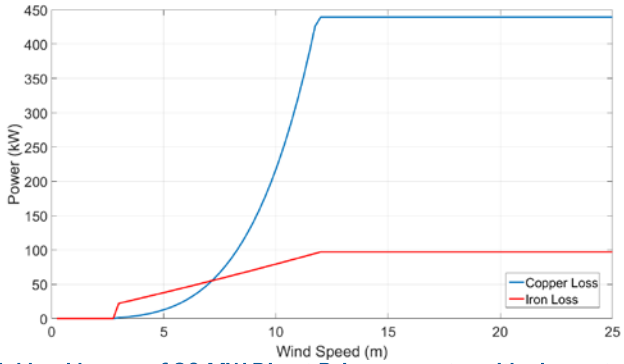

Figure 4-7 Partial load losses of 20 MW Direct-Drive generator with shear stress of 40 kN/m².

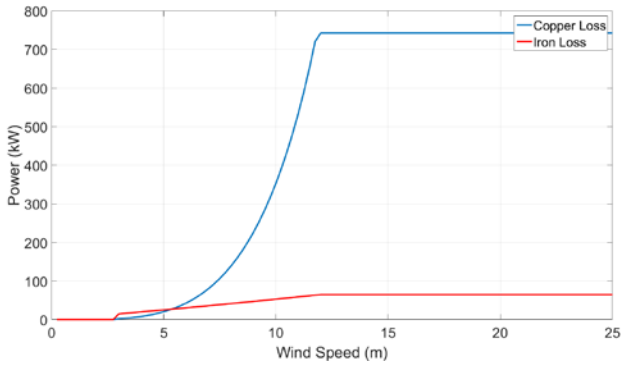

Figure 4-8 Partial load losses of 20 MW Direct-Drive generator with shear stress of 60 kN/m².

These losses result in efficiency curves as presented in Figure 4-8.

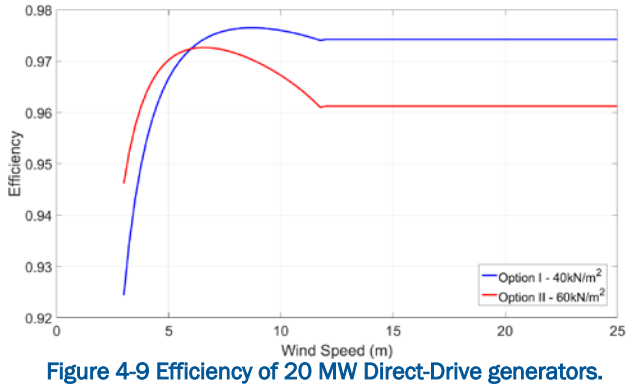

Figure 4-9 Efficiency of 20 MW Direct-Drive generators.

4.4.1.1 Size

20 MW		
Option I	D_{gen} = 14 m	L_{gen} = 2.25 m
Option II	D_{gen} = 14 m	L_{gen} = 1.50 m

4.4.1.2 Weight

20 MW

Option I	$m_{gen,active}$ ~ 135 ton	$m_{gen,total}$ ~ 572 ton
Option II	$m_{gear,active}$ ~ 90 ton	$m_{gen,total}$ ~ 527 ton

The weight of the support structure is assumed to be equal to that of the superconducting Direct-Drive generator.

4.4.1.3 Cost

20 MW

Option I	$C_{gen,active}$ ~ 1.73 M€	$C_{gen,structure}$ ~ 1.31 M€	$C_{gen,total}$ ~ 3.04 M€
Option II	$C_{gen,active}$ ~ 1.16 M€	$C_{gen,structure}$ ~ 1.31 M€	$C_{gen,total}$ ~ 2.47 M€

4.4.1.4 AEP and efficiency

20 MW

Option I	AEP = 97.3 GWh/year	AEP_0 = 99.0 GWh/year
Option II	AEP = 97.0 GWh/year	

4.4.1.5 LCoE

20 MW

Option I	$\Delta LCoE/ LCoE_0$ = -1.45 %
Option II	$\Delta LCoE/ LCoE_0$ = -1.39 %

4.4.2 Medium Speed Drive train Performance

The partial loads losses of the 20 MW medium speed drive train is shown in Figure 4-9.

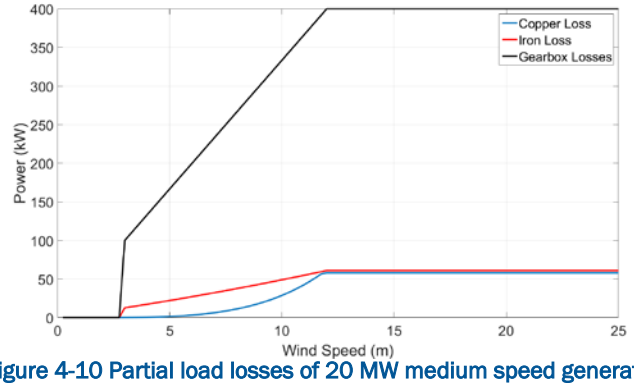

Figure 4-10 Partial load losses of 20 MW medium speed generator.

These losses result in efficiency curves as presented in Figure 4-10.

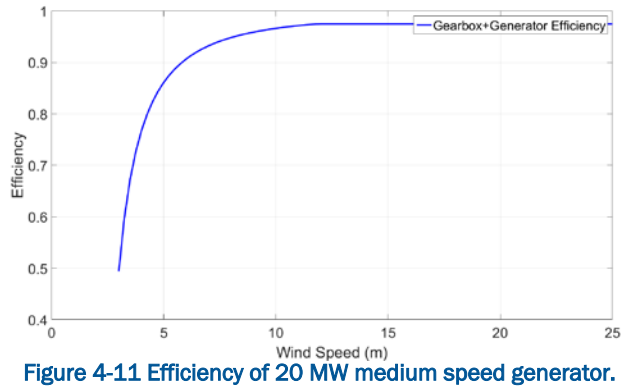

Figure 4-11 Efficiency of 20 MW medium speed generator.

4.4.2.1 Size

20 MW D_{gen} = 1.1 m L_{gen} = 1.9 m

4.4.2.2 Weight

20 MW $m_{gen,active}$ ~ 41.5 ton $m_{gen,total}$ ~ 83 ton
M_{gear} ~ 362 ton $m_{drive,total}$ ~ 445 ton

The weight of the support structure is assumed to be equal to that medium speed generator (Polinder, Van der Pijl, De Vilder, & Tavner, 2006).

4.4.2.3 Cost

20 MW $C_{gen,active}$ ~ 0.30 M€ $C_{gearbox}$ ~ 4.34 M€
$C_{gen,structure}$ ~ 0.12 M€ C_{total} ~ 4.76 M€

4.4.2.4 AEP and efficiency

20 MW AEP = 96.6 GWh/year AEP_0 = 99.0 GWh/year

4.4.2.5 LCoE

20 MW $\Delta LCoE/ LCoE_0$ = 0 % (Used as reference drive train)

5 COMPARISON OF DRIVE TRAINS

In order to compare the INNWIND.EU drive trains, the mechanical power curve of the INNWIND.EU reference turbines in Figure 5-1 are used to calculate the Annual Energy Production (AEP) by also assuming that the turbines are positioned in an IEC wind class Ia with an average wind speed of v_{ave} = 10.0 m/s. The rotation speed curves of the turbines are shown in Figure 5-2.
The partial load efficiency of the generator and the power converter of deliverable report D3.31 are used to correct for the losses of the specific drive trains in the integration (Deng, et al., 2015). This method is described in details in deliverable report D3.11 on the superconducting generators (Abrahamsen, Liu, & Polinder, 2017).

Figure 5-4 is showing the partial load efficiency of the INNWIND.EU drive trains as well as the Weibull wind distribution of the wind class Ia. The integration of the annual energy production is performed from zero wind speed in case of the superconducting generators, because the power consumption of the cryogenic cooling system is included, and from the cut-in wind speed $V_{cut\text{-}in}$ = 4 m/s for the remaining drive train. The upper limit of the integration when including the losses is the rated wind speed V_{rated} = 11.4 m/s, because above rated then the turbine blades are pitched a bit different in order to compensate for the losses. Thus full power production is integrated from V_{rated} to the cut-out wind speed at $V_{cut\text{-}out}$ = 25 m/s.

Figure 5-5 and Figure 5-6 are showing the partial load efficiencies of the INNWND.EU 10 MW and 20 MW for wind speeds between cut-in and rated together with the Weibull wind speed distribution.

It is clearly seen that the magnetic Pseudo Direct Drive (PDD) generator is the most efficient drive train for all wind speeds for both at 10 MW and 20 MW. The superconducting direct drive generators are shown with different constant power consumption for running the cryogenic cooling equipment. For the 10 MW MgB_2 generator a consumption of 50 kW and 100 kW are shown. The latter is the estimated consumption found by projecting the SupraPower cryostat and cooling technology running at T = 20 K (Sun, Sanz, & Neumann, 2015) onto the INNWIND.EU MgB_2 generator (Abrahamsen, Liu, & Polinder, 2017) . By comparing to the reference drive trains, then it is seen that the Permanent Magnet Direct Drive (PMDD) provides higher efficiencies, but the MgB_2 generator can be more efficient than the medium speed drive train if the power consumption is reduced to 50 kW or 0.5 % of rated power. This should be considered as a target for future designs. The partial load efficiency of the high temperature superconducting generator does not include the power consumption for the cooling system, but a preliminary analysis in Deliverable report D3.12 is indicating 15 kW (Thomas & Azar, 2016). This power consumption has not been included in the efficiency curve, because the cryogenic design is preliminary.

The analysis of the 20 MW superconducting MgB_2 generator is very similar to the 10 MW analysis and show that the MgB_2 generator falls in between the Permanent magnet direct drive and the medium speed drive train if the constant cooling power is limited to 100 kW or again 0.5 % of rated power. The estimated power consumption for cooling of 263 kW is too high and will have to be reduced in future designs.

In the previous sections, the annual energy production (AEP) of the different drive trains was listed as well as the ideal Annual Energy Production (AEP_0), where all electrical losses (generator and power converter) are neglected. In this way the ratio of the specific AEP to the ideal AEP_0 is showing the remaining margin for improvement.

Table 5-1 is showing the annual energy production (AEP) as well as the cost of the different drive trains of the INNWIND.EU project. The annual energy production AEP is also related to the ideal annual energy production without losses AEP_0 by calculating (AEP - AEP_0)/ AEP_0. This number is showing how far the different drive train technologies are from the loss free case. The difference between two drive train will result in the same difference in the Levelized Cost of Energy using the sensitivity analysis method described in deliverable D3.11 (Abrahamsen, Liu, & Polinder, 2017):

$$\frac{\Delta LCoE}{LCoE_0} = -\frac{\Delta E_{i,c}}{E_{i,c0}} + \frac{LCoE_{CAPEX}}{LCoE_0}\left(\frac{\Delta C_D}{C_{D,0} + C_{R,0}} + \frac{\Delta C_R}{C_{D,0} + C_{R,0}} - \frac{\Delta a}{a_0} - \frac{\Delta LT}{LT_0}\right) + \frac{LCoE_{OPEX}}{LCoE_0}\left(\frac{\Delta O_{D,C}}{O_{D,C0}+O_{R,C0}} + \frac{\Delta O_{R,C}}{O_{D,C0}+O_{R,C0}}\right) \quad (5\text{-}1)$$

where the first term is the relative change in annual energy production $E_{i,c}$, the second and last term is related to CAPital Expenditure (CAPEX) and Operational Expenditure (OPEX). The cost of the drive trains is denoted C_D and the rest of the turbine and foundation cost is denoted C_R. The Operation and maintenance cost of the drive train is denoted $O_{D,C}$ and similar for the rest of the turbine and foundation $O_{R,C}$. the parameter *a* is related to the interest rate *w* of investments in the energy sector and *LT* is the life time of the structure assumed to be 25 years.

The ratio between CAPEX and OPEX contribution to the Levelized Cost of Energy has been found to be $LCoE_{CAPEX} / LCoE_{0\_10MW} \sim 0.72$ and $LCoE_{OPEX\_10MW} / LCoE_0 \sim 0.28$ for the 10 MW INNWIND.EU reference turbine (Abrahamsen, Liu, & Polinder, 2017). For the 20 MW turbine these ratios are expected to be $LCoE_{CAPEX\_20MW} / LCoE_0 \sim 0.76$ and $LCoE_{OPEX\_20MW} / LCoE_0 \sim 0.24$ (see table 3.2 in (Abrahamsen, Liu, & Polinder, 2017)).

The above method has been used to evaluate the impact in the LCoE due to the INNWIND.EU drive trains compared to the 2 stage gear box with a medium speed generator, which is the reference drive train of INNWIND.EU. The results are shown in Table 5-1 for the 10 MW and in Table 5-2 for the 20 MW drive trains.

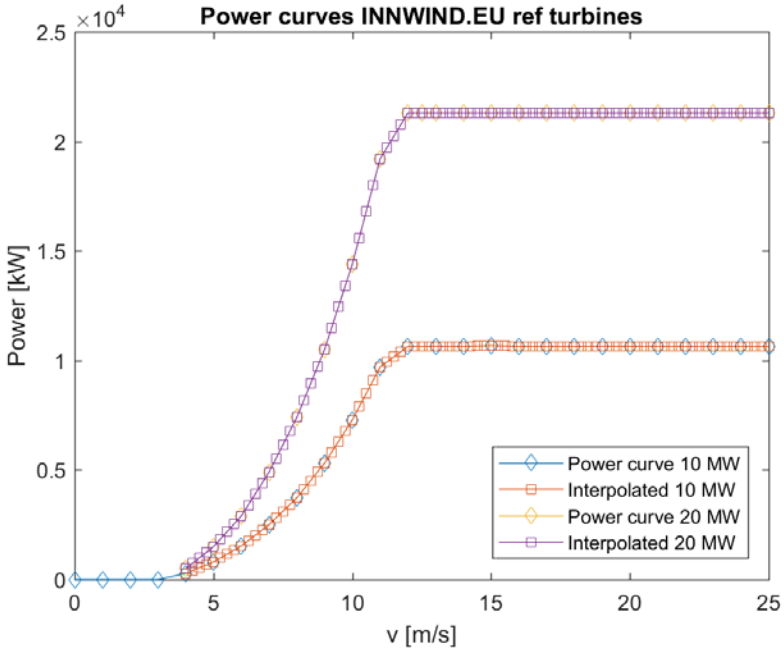

Figure 5-1 Mechanical power curves of the INNWIND.EU reference turbines used for the calculation of the annual energy production when the turbines are placed in a IEC wind class Ia with an average wind speed of 10 m/s and a shape parameter of k = 2.

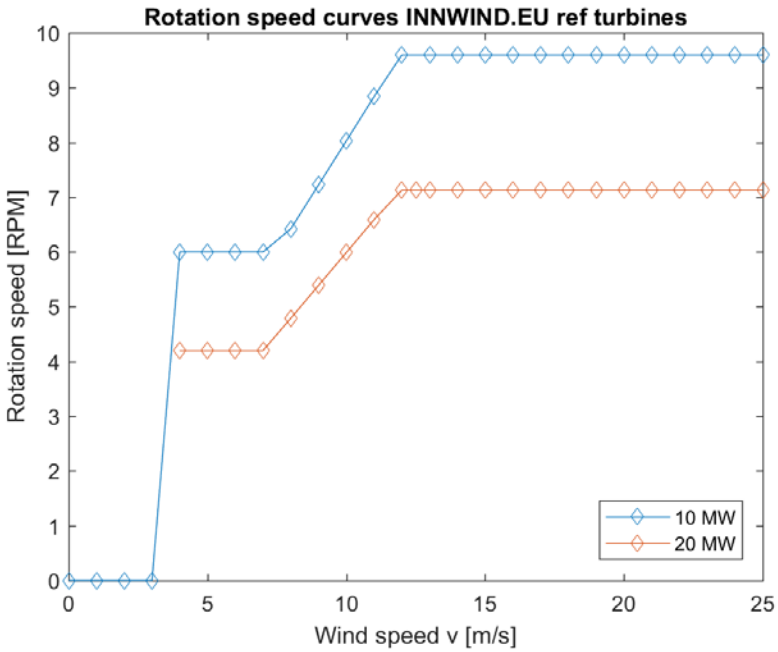

Figure 5-2 Rotor rotation speed as function of wind speed of the INNWIND.EU reference turbines.

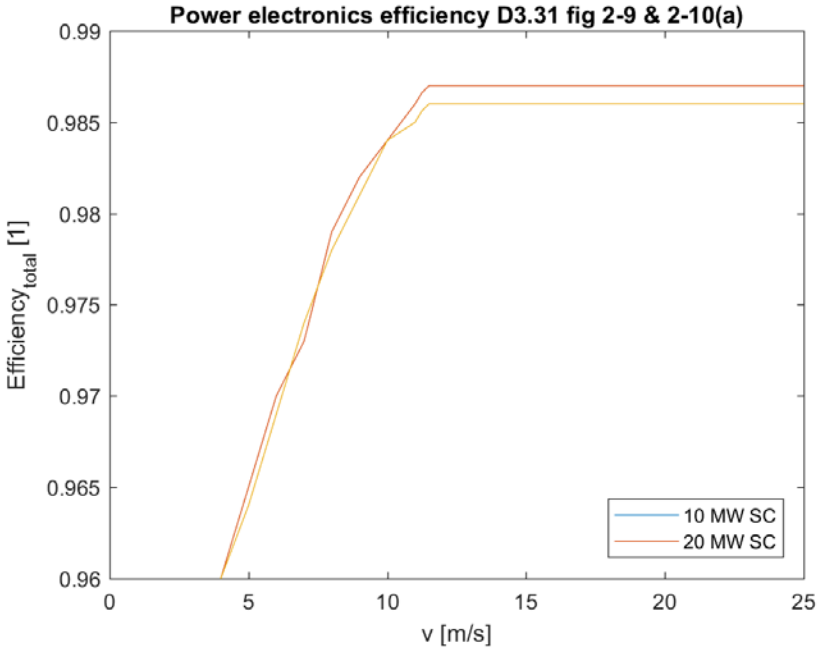

Figure 5-3 Partial load efficiency of the power converters tailored for the INNWIND.EU drive trains at 10 MW and 20 MW. The curves are reproduced from fig 2-9 (a) and fig 2-10(a) of deliverable report D3.31 (Deng, et al., 2015). The curves are representing a back-to-back voltage source converter tailored for the superconducting generators, but it is also applied to the Pseudo Direct Drive (PDD) generators as well as the reference drive trains, because it is considered as the most industrial established technology.

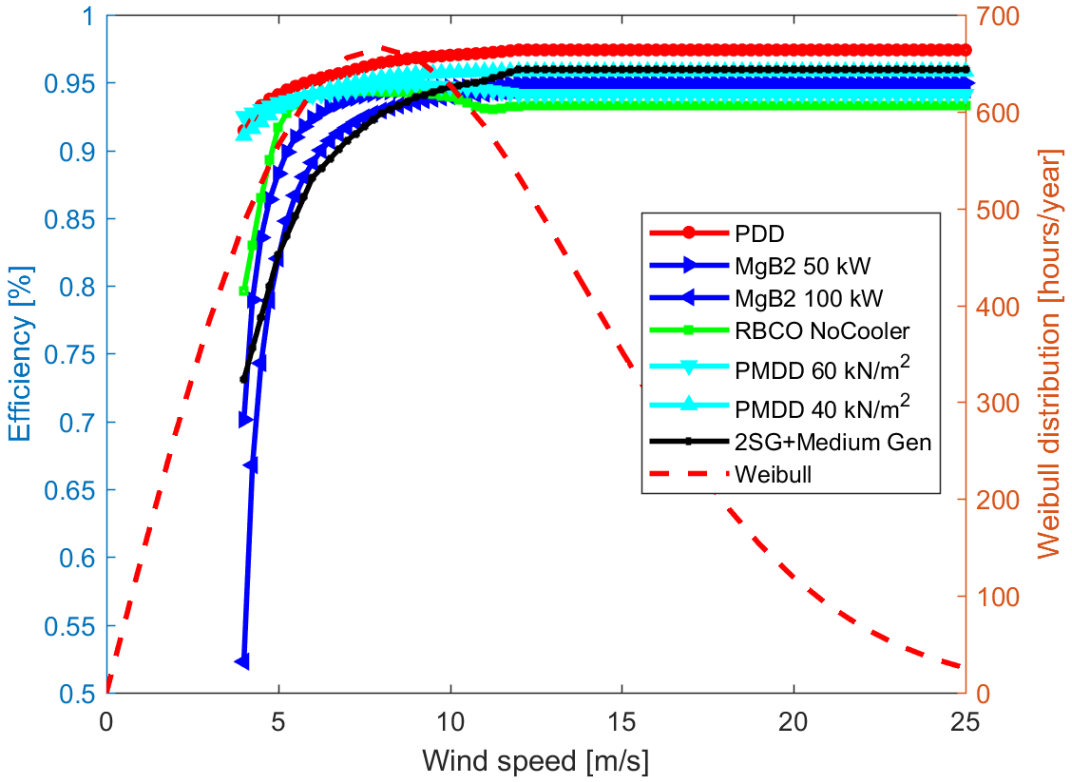

Figure 5-4 Comparison of partial load efficiency of the 10 MW INNWIND.EU drive trains as function of wind speed. The Weibull wind speed distribution for a wind Class Ia is used to calculate the annual energy production. The Pseudo Direct Drive (PDD) generator shows the highest efficiency. The MgB_2 direct drive generators are shown with a constant cryogenic cooling power consumption of 50 kW and 100 kW respectively. The efficiency curve of the RBCO generator is shown without the cryogenic power consumption. Two Permanent Magnet Direct Drive (PMDD) generators with a shear force density of 40 and 60 kN/m² is also shown as well as a 2 stage gear box combined with a medium speed generator (2SG+Medium Gen). It should be noted that the partial load efficiency of the power converted is included the in the curves shown in this figure.

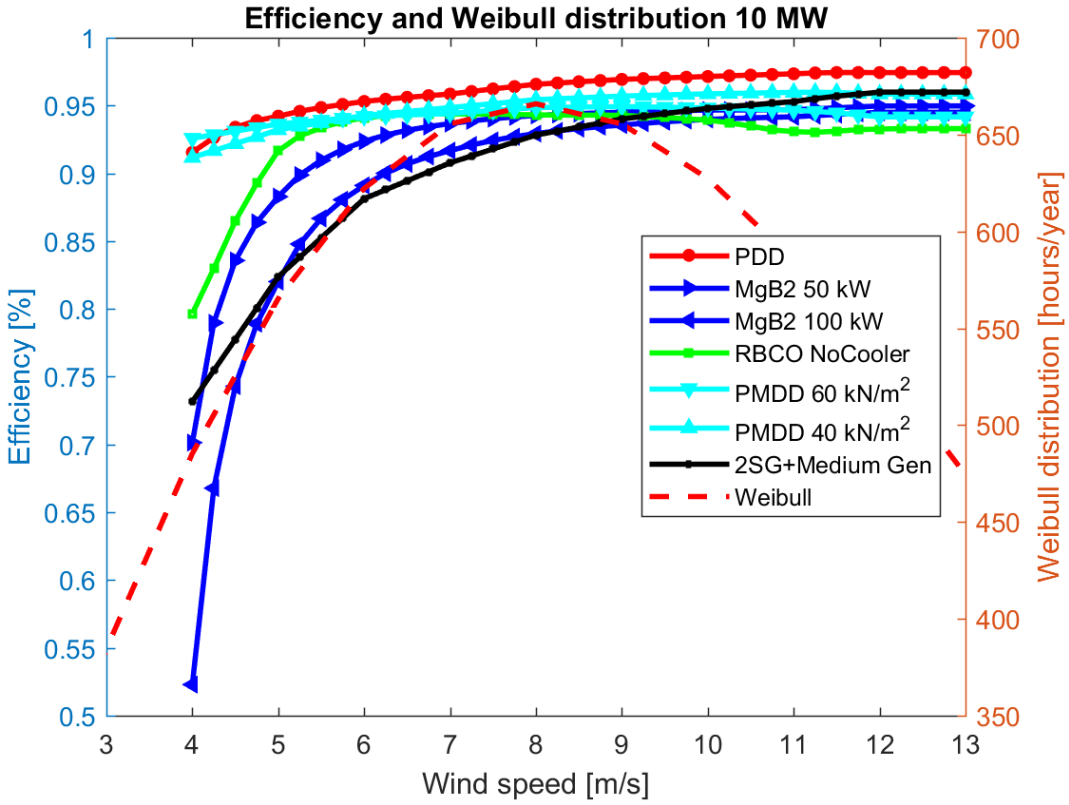

Figure 5-5 Efficiency of 10 MW INNWIND.EU drive trains only shown from cut-in to rated wind speed from the plot on Figure 5-1. It is seen that the PDD has the highest efficiency for all wind speeds. The superconducting direct drive generator efficiencies are below the permanent magnet direct drive (PMDD) generators, but can be more efficient than the medium speed drive train (2SG+Medium Gen), if the power consumption for the cryogenic cooling system is limited to below 50 kW for the 10 MW MgB2 direct drive generator (MgB2 50 kW).

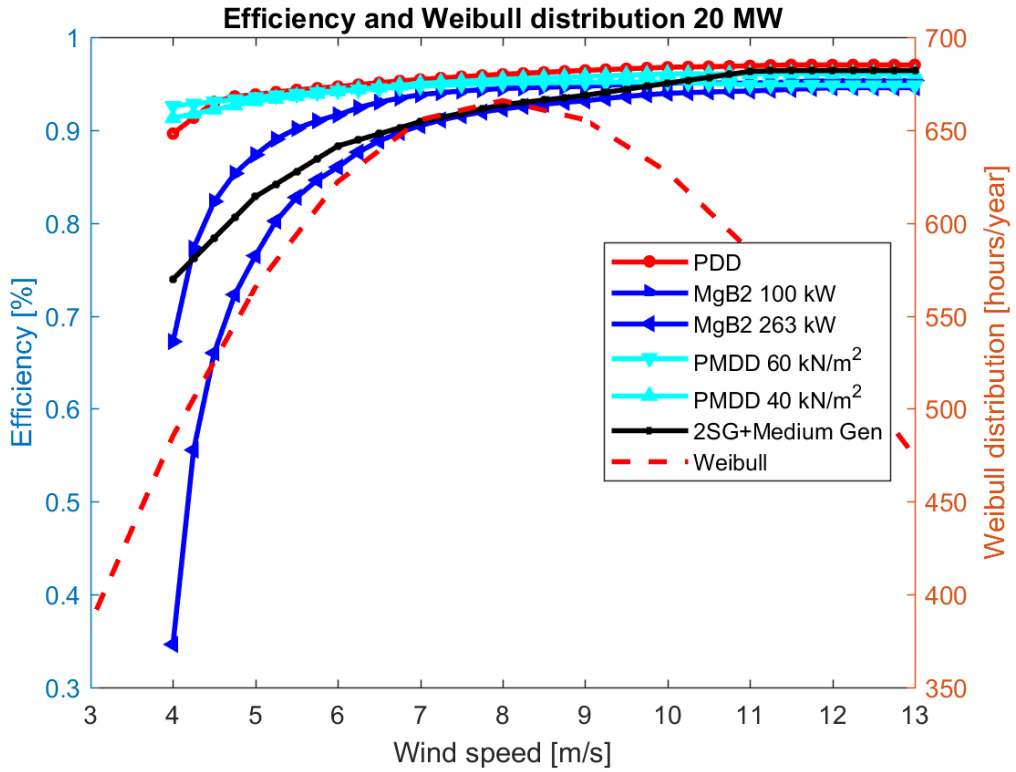

Figure 5-6 Efficiencies of the 20 MW INNWIND.EU drive trains shown from cut-in to rated wind speed. The PDD is again showing the highest efficiency for all wind speeds, but it is quite close to the Permanent Magnet Direct Drive (PMDD) generators with shear forces of 40 and 60 kN/m². Two 20 MW MgB2 superconducting generators are shown with a constant power consumption of 100 and 263 kW respectively. The latter is the estimated power consumption of the INNWIND.EU 020 MW MgB_2 direct drive generator, but in order to be comparable to the medium speed drive train then it would be beneficial to reduce the cryogenic power consumption to the proposed 100 kW.

Drive train – 10 MW	AEP [GWh/year]	Cost [M€]	$(AEP- AEP_0)/AEP_0$	$\Delta LCoE/LCoE_{Medium}$
PDD	49.2	1.13	-1.3 %	- 1.91 %
MgB_2 – 50 kW	48.6	1.60	-2.5 %	- 0.21 %
MgB_2 - 100 kW	48.3	1.72	-3.1 %	+ 0.52 %
RBCO	48.5	0.76*	-2.6 %	- 1.01 %
PMDD 40 kN/m²	48.9	1.01	-1.8 %	-1.52 %
PMDD 60 kN/m²	48,7	0.85	-2.2 %	-1.32 %
Medium speed	48.5	1.65	-2.6 %	Ref drive train

Table 5-1 Comparison of Annual Energy Production(AEP) and Cost of the 10 MW INNWIND.EU drive trains and selected reference drive trains: Pseudo Direct Drive (PDD), Superconducting MgB_2 direct drive with 50 kW and 100 kW power consumption for the cryogenic cooling, High temperature superconducting RBCO coated conductor direct drive (RBCO), Permanent Magnet Direct Drive with shear force density of 40 kN/m² and 60 kN/m² (PMDD), 2 stage gearbox with medium speed generator (Medium speed).*Does not include the cost of the cryogenic cooling system, but is expected to increase the cost by 30 %. The annual energy production without losses is estimated to be AEP_0 = 49.8 GWh/year. The cost of the rest of the structure is assumed C_R = 25.0 M€.

Drive train – 20 MW	AEP [GWh/year]	Cost [M€]	$(AEP- AEP_0)/AEP_0$	$\Delta LCoE/LCoE_{Medium}$
PDD	97.6	2.30	- 1.45 %	- 2.05 %
MgB_2 - 263 kW	95.7	3.98	- 3.31 %	+ 0.55 %
RBCO	-	1.41*	-	-
PMDD 40 kN/m²	97.3	3.04	- 1.74 %	- 1.45 %
PMDD 60 kN/m²	97.0	2.47	- 2.03 %	-1.39 %
Medium speed	96.6	4.76	- 2.45 %	Ref drive train

Table 5-2 Comparison of Annual Energy Production(AEP) and cost of the 20 MW INNWIND.EU drive trains and selected reference drive trains: Pseudo Direct Drive (PDD), Superconducting MgB_2 direct drive with 263 kW power consumption for the cryogenic cooling, High temperature superconducting RBCO coated conductor direct drive (RBCO), Permanent Magnet Direct Drive with shear force density of 40 kN/m² and 60 kN/m² (PMDD), 2 stage gearbox with medium speed generator (Medium speed).*Does not include the cost of the cryogenic cooling system, but is expected to increase the cost by 30 %. The annual energy production without losses is estimated to be AEP_0 = 99.0 GWh/year. The cost of the rest of the structure is assumed C_R = 52.9 M€.

5.1.1 Mass of drive trains and mass scaling

The masses of the different drive trains are shown in Figure 5-7. It is clearly seen that the Pseudo Direct Drive (PDD) is providing a lower mass than the reference drive trains outlined in this report. The superconducting MgB_2 direct drive generators are heavy in comparison to the reference drive trains as a result of minimizing the usage of superconducting wire to reduce the cost.

Figure 5-8 is showing the mass scaling of the PDD as reported in Deliverable 3.21 (Penzkofer & Atallah, 2015) and the superconducting MgB_2 generator as function of the turbine rotor diameter. The drive train mass of the PDD have since been updated to m_{PDD} ~ 420 ton, which is 100 tons less than shown in Figure 5-8. The blade mass and also the nacelle mass has been included in order to provide an estimate of the Rotor Nacelle Assembly (RNA) mass of the INNWIND.EU drive trains. For comparison then the expected RNA mass of the INNWIND.EU reference turbines are included with stars. A previous 10 MW Permanent Magnet Direct Drive generator design by Polinder in 2007 with m_{PMDD} ~ 325 ton has also been included for comparison of the mass of the MgB_2 generator (Polinder H. , 2007). As indicated by Figure 5-7, the PMDD is expected to have improved and will provide a lower weight. The rotor scaling has also been done to lower rotor diameters and the RNA mass has been compared to the Vestas V-164 turbine shown as a pentagon (de Vries, 2013).

It is seen that the Pseudo Direct Drive is providing a substantial better scaling of the RNA mass than the INNWIND.EU reference turbine, whereas the MgB_2 superconducting direct drive is only scaling slightly better than the reference turbines. Thus the PDD is providing an innovative drive train technology with a mass scaling beating the expected scaling of the reference drive train. The MgB_2 superconducting direct drive generator is providing a disappointing mass scaling, which is a result of minimizing the cost of the generator, by removing superconductor and increasing the amount of steel laminates in the machine. This design philosophy of “cheap and not too heavy” has been shown not to work and future design philosophies most likely will have to rely on optimization methods where the generator mass can be restricted as a constraint. Secondly it has been shown that more powerful and cheap superconductors will most likely be needed in order to identify the superconductor generator topology that can compete with the present drive trains in terms of both cost and weight.

However a simple check of the economical feasibility of a superconducting wind turbine generator design was proposed in D3.11 (Abrahamsen, Liu, & Polinder, 2017). Compare the cost of the superconductors, the cryostat and the cooling system directly to the cost of 4-6 tons of $R_2Fe_{14}B$

Permanent magnet material for a 10 MW (Table 4-2) and 12-18 tons for a 20 MW direct drive generator (Table 4-3). One would have to decide on the unit cost of the $R_2Fe_{14}B$ Permanent magnet material depending on the source, but during the INNWIND.EU project proposed values have decreased from C_{PM} > 150 €/kg to a the current level of about $C_{PM,2017}$ ~ 25 €/kg.

For the 10 MW generator the cost of 4 tons of Permanent Magnets will only be 100 k€. Comparing this to the 10 MW SC generator, then if the MgB_2 wire cost is reduced by a factor of 4 then the cost of the MgB_2 wire will be about 20 k€ and then the cryostat and cooling system can only cost about 80 k€. This is a considerable reduction compared to the current estimate of the cryostats and cooling system adding up to 600 k€. The questions is therefore if wind industrialization of the manufacturing of the cryostats and cooling systems can drive the cost down by a factor of almost 10? Finally the power consumption of running the cooling system will also give a penalty on the Levelized cost of Energy and have to be considered.

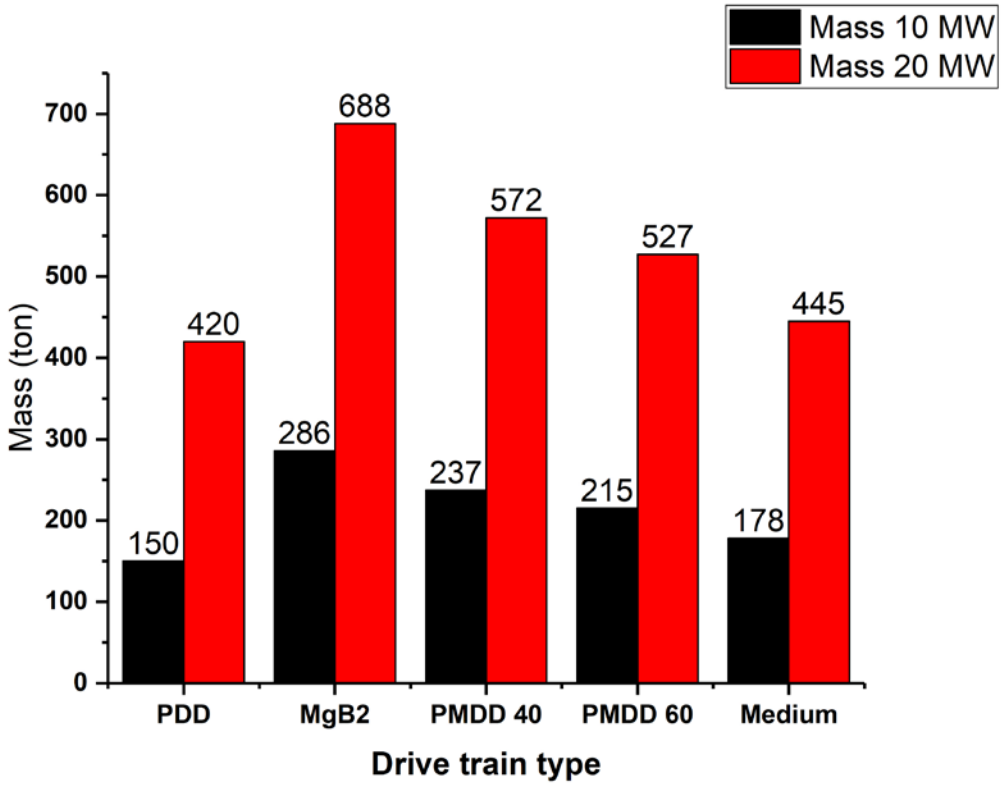

Figure 5-7 Drive train masses of INNWIND.EU wind turbine generators as integrated into the INNWIND.EU nacelle compared with predicted mass of reference drive trains as given in this report. It is seen that the PDD is providing a lower mass than all the reference drive trains, whereas the superconducting direct drive generator provides the highest mass as result of reducing the usage of superconducting wire the drive train.

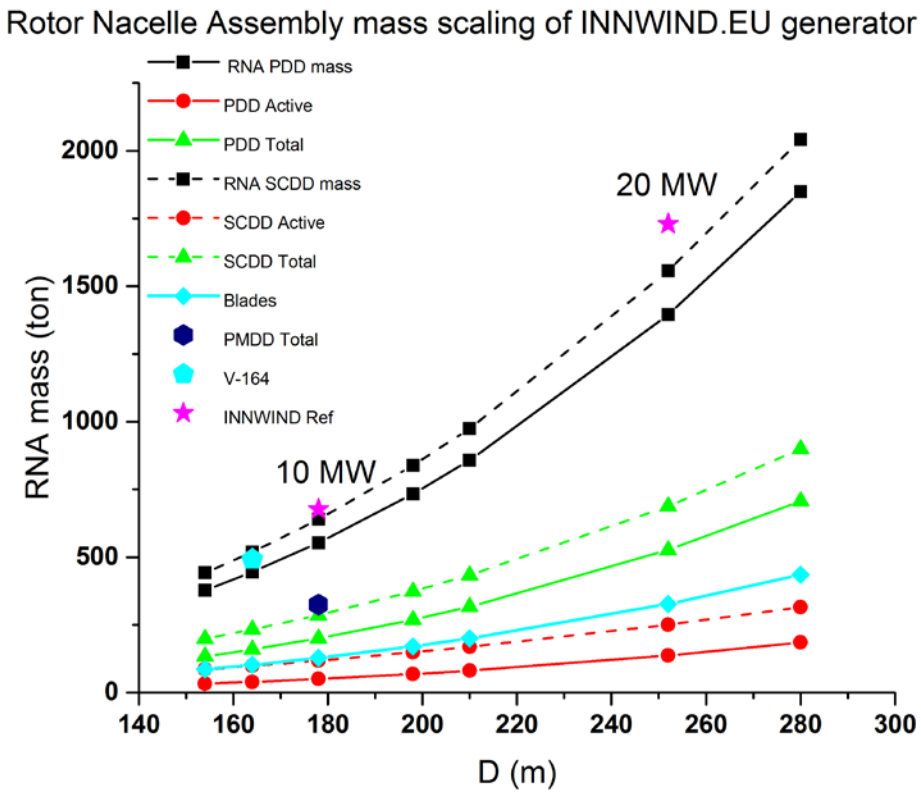

Figure 5-8 Mass scaling of the Rotor Nacelle Assembly (RNA) mass as function of the rotor diameter of the INNWIND,EU turbines with either a MgB_2 front mounted direct drive generator (SCDD) or a front mounted magnetic Pseudo Direct Drive generator (PDD). The Rotor Nacelle assembly mass is given as the sum of the blades, the total generator mass and the nacelle mass (not shown). The RNA mass scaling of the INNWIND.EU reference turbines are shown with stars for a 10 MW and 20 MW rotor for comparison. Secondly the RNA mass of the Vestas V-164 turbine is indicated as well as the total generator mass of a Permanent Magnet Direct Drive (PMDD) generator. It is clearly seen that the PDD provides a better mass scaling than the SCDD.

6 CONCLUSION

The INNWIND.EU project has investigated the innovative drive train technologies: Pseudo Direct Drive and Superconducting direct drive as part of work package 3 electromechanical conversion. The two drive train technologies have been integrated into an innovative nacelle based on a static King-pin holding a hub with two main bearing placed on each side of the hub. The generators we placed in front of the turbine blades in order to provide the possibility to replace the drive train without removing the turbine rotor. Finally the PDD and superconducting generators were integrated with power converters in order to be interfaced to the electrical grid.

This report collects all the performance indicators in terms of size, weight, cost, efficiency and impact on Levelized Cost of Energy.

It is concluded that the Pseudo Direct Drive (PDD) generator technology is providing superior properties in all performance indicators compared to the reference drive trains examined as well as the INNWND.EU reference turbines. Thus the PDD is providing an innovative generator technology, which is scaling considerable better than current drive train technologies.

It is also concluded that the superconducting direct drive generator technology cannot outperform the reference drive trains. It is found that the Permanent Magnet Direct Drive (PMDD) generator technology is expected to be better than the proposed superconducting direct drive generator technology in terms of efficiency and cost, which is resulting in a better LCoE of the PMDD than the superconducting. The weight and size of the PMDD are comparable to the superconducting direct drive, but with the weight of the PMDD being somewhat lower than the superconducting generator. The superconducting direct drive generator seems to be able to provide efficiencies and cost similar to a 2 stage gearbox with a medium speed generator. Further work will however be needed to optimize the power consumption of the cryogenic cooling system to a level of about 0.5 % of rated power before the partial load efficiency becomes better than the medium speed drive train.

It has been found that more light weight superconducting generator topologies will most likely become more feasible than the heavy iron cored topology used in the INNWIND.EU project, if cheaper (4 times) and more powerful (4 times the critical current density) MgB_2 wires will become available in the future. The reduction of the cost of the high temperature superconductors is also needed for them to open for more light weight generator topologies.

Finally it should be said that the cost of the $R_2Fe_{14}B$ Permanent Magnet material as well as the superconductors have a large influence on the economical feasibility of the drive trains investigated in the INNWIND.EU project. There has been no attempt to analyse the sensitivity of the INNWIND.EU conclusion with respect to raw material availability and cost. Thus the current conclusions constitute the situation in 2017, but we believe that future analysis can be done based on the INNWIND.EU work by updating the assumptions of the unit cost of the generator materials.

7 REFERENCES

Polinder, H. (2007). 10 MW wind turbine direct-drive generator design with pitch or active speed stall control. *Electric Machines & Drives Conference, 2007. IEMDC'07. IEEE International. Vol. 2. IEEE, 2007.*

Abrahamsen, A., & Jensen, B. (2012). Design study of coated conductor direct drive wind turbine generator for small scale demonstration. *European Conference on Applied Superconductivity (EUCAS)* (pp. 753 – 758). Physics Procedia 36 (2012) 753 – 758.

Abrahamsen, A., Jensen, B., Seiler, E., Mijatovic, N., Rodriguez-Zermeno, V., Andersen, N., & Østergård, J. (2011). Feasibility study of 5 MW superconducting wind turbine generator. *Physica C 471*, 1464–1469.

Abrahamsen, A., Liu, D., & Polinder, H. (2017). *Direct drive superconducting generators for INNWIND.EU wind turbines.* INNWIND.EU deliverable report D3.11.

Atallah, K., & Penzkofer, A. (2015). *Analytical models for magnetic gears and Pseudo Direct-Drive machines PDD®.* INNWIND.EU workpackage meeting Pamplona 19/10-2015.

Bauer, M. (2017). Status of the Ecoswing project. *EUCAS 2017*, (pp. 2LO2-01). Geneve.

Columbus Superconductors. (2017, October). *Columbus Superconductor website*. Retrieved from http://www.columbussuperconductors.com/

de Vries, E. (2013, september 9). Close up - Vestas V164-8.0 nacelle and hub. *Wind Power Mountly.*

Deng, F., Chen, Z., Karwatzki, D., Mertens, A., Parker, M., & Finney, S. (2015). *Converter designs tailored to SC and PDD concepts.* INNWIND.EU deliverable report D3.31.

Grasso, G. (2017, October). Privat communication.

Guan, Y., & et. al. (2017). Comparison of Electromagnetic Performance of 10MW Superconducting Generators with Different Topologies for Offshore Direct-Drive Wind Turbines. *IEEE transaction on applied Superconductivity*.

Magnusson, N., Hellesø, S., Paulsen, M., Eliassen, J., & Abrahamsen, A. (2016). *Fabrication of MgB2 Coils – A superconducting generator pole demonstrator.* INNWIND.EU deliverable report D3.13.

Penzkofer, A., & Atallah, K. (2015). *Design and PI of PDD generator.* INNWIND.EU Deliverable report D3.21.

Polinder, H., Van der Pijl, F., De Vilder, G., & Tavner, P. (2006). Comparison of direct-drive and geared generator concepts for wind turbines. *IEEE Transactions on energy conversion, 21(3)*, 725-733.

Stehouwer, E., van Zinderen, G., & Hossain, S. (2017). *Conceptual nacelle designs of 10-20 MW wind turbines.* INNWIND.EU deliverable report D3.41.

Sun, J., Sanz, S., & Neumann, H. (2015). Conceptual design and thermal analysis of a modular cryostat for one single coil of a 10 MW offshore superconducting wind turbine. *IOP Conf. Series: Materials Science and Engineering, 101*, 012088.

Thomas, A., & Azar, Z. (2016). *Summary Report for Work Package 3.1.2 – Investigation of HTS Super-Conducting Direct Drive Generators.* INNWIND.EU deliverable report D3.12.

8 APPENDIX: MGB_2 WIRE QUALIFICATION TEST

The MgB_2 coil demonstration of D3.13 (Magnusson, Hellesø, Paulsen, Eliassen, & Abrahamsen, 2016) has shown that 8 out of 10 double pan cake coils have small segments with a length between 1 to 36 cm, where the superconducting properties are considerable weaker than the remaining 500 m of MgB_2 tape in each pan-cake coil.

The dilemma of winding superconducting coils is always that one will have to measure the superconducting properties of the initial wire before winding if any manufacturing issues from the wire manufacturer should be identified. In the case of relatively cheap superconductors and low critical temperatures such as MgB_2 and also NbTi with unit cost of ~ 4 €/m and ~ 0.4 €/m, one would have to pay much more for the wire testing than for the wire itself. In these cases it is often said that testing the wire is as expensive as to wind the coil product and test if the coil works. If MgB_2 should be used for a wind turbine generator then they have to be cheap and there will not be economical room for pre-winding testing. The winding of the 10 double pancake coils of the INNWIND.EU project was therefore seen as a test if the wire was mature enough to be wound without prior wire testing.

The 5 km of MgB_2 wire used by SINTEF for the race track coil winding was delivered on spools with a diameter of 0.8 m and with about 1 km of MgB_2 wire on each spool. It was agreed with the wire manufacturer Columbus Superconductors (Columbus Superconductors, 2017) that a piece of 10-20 cm at each spool end were tested in applied magnetic fields up to B = 1.8 Tesla and at temperatures T = 10, 16 and 20 K. This was done in a separate cryostat at Columbus and the measured properties have been reported in D3.13 (Magnusson, Hellesø, Paulsen, Eliassen, & Abrahamsen, 2016).

It is clear from the measurements of the MgB_2 race track coil that a method for investigating longer length of MgB_2 wire will be beneficial for further development of MgB_2 coils. It was decided to design a wire qualification test at DTU Wind Energy, where a length of up to 1/10 of the pancake wire length could be tested for weak superconducting segments.

The wire qualification test was designed to address the following issues:

1) Is the minimum bending diameter of $D_{Critical\ bend}$ = 150 mm constant along longer piece lengths of the wire?
2) Will a simple winding procedure introduce the weak segments in the wire by unintentional damage during the handling?
3) Will the race track coil shape introduce damages to the wire, which are not seen for round coils?
4) How long a wire length can be wound into a coil shape and tested within a reasonable time?

In order to address the above questions it was decided to construct a race track coil former with an opening given by the critical bending diameter D_{end} = 150 mm and with a straight section of 100 mm. The cross section area of the coil was set to a width of 30 mm x thickness of 10 mm corresponding to 10 windings across the width and about 10 windings along the thickness, since the wire dimensions are 3.0 mm wide and 0.7 mm thick (with the allowance of some air then an effective wire thickness of 1 mm is expected). One turn is approximately L_{turn} ~ 0.67 cm and the 100 turns would then allow 67 m of wire to be tested. Figure 8-1 shows the dimensions of the coil former.

The intension of the wire qualification test is to wind up about 50 m of wire onto the coil former, cool it down to T = 20-30 K and measure if the resistance of the wire is dropping to zero. If that is not the case then damages in form of fully resistive segments are present. If the resistance is dropping to zero then the current of the coil should be ramped up to about 1/10 of the critical current in order to measure the IV curve of the superconductor. If the wire includes weak

segments then the voltage drop of the winding is expected to be describes by two power-law functions: one for the weak segment and one for the good superconductor

$$U_{coil} = E_0 L_{weak} \left(\frac{I}{I_{C,weak}}\right)^{n_{weak}} + E_0 L_{good} \left(\frac{I}{I_{C,good}}\right)^{n_{good}} + U_0 \quad (8\text{-}1)$$

where I is the current running through the coil, E_0 is defined as the electric field of 10^{-4} V/m along the superconductor, when the current is equal to the critical current I_C. The power law exponent n is quantifying how abrupt the transition from the low loss state with $I < I_C$ to the loss state of $I > I_C$ is taking place. The length of the weak segment is given by L_{weak}, the length of the good segment is given by L_{good} and the entire wire length is $L_{wire} = L_{weak} + L_{good}$. The constant voltage U_0 is the thermo-voltage resulting from different metals soldered together in the electrical circuit connected to the voltmeter.

In the case of the INNWIND.EU MgB_2 pan cake coils, it was found that the good superconducting wire part was described by $I_{C,\,good}$ ~ 140 A at T = 20 K and the power law exponent was n_{good} ~ 20 in wire lengths of L_{good} ~ 500 m. The weak segment is described by $I_{C,\,weak}$ ~ 1-40 A at T = 20 K and the power law exponent was n_{weak} ~ 1-3 in wire lengths of L_{weak} ~ 1-36 cm (see chapter 5.3.2 in deliverable 3.11 (Abrahamsen, Liu, & Polinder, 2017)). If such similar weak segments are present in the wire qualification test then the low power-law exponent would result in a considerable voltage drop even at low coil currents. Thus the wire qualification test can be used to investigate if the weak segments of the MgB_2 race track coil can be reproduced and thereby hopefully also to specify how to avoid the weak segments in the future.

A cryostat for cooling the MgB_2 coils was borrowed from the Department of Electrical Engineering at DTU as shown in Figure 8-2. It is equipped with a power full CH-110 cold head and F-70 Helium compressor from Sumitomo, whereby cooldown to T = 25 K should be possible within some hours.

The initial wire qualification test should not be performed to the full critical current of the MgB_2 wire, because the winding will need impregnation with epoxy or bee-wax in order to obtain thermal and mechanical stability at full current. The coil former is however designed to undergo a subsequent impregnation, whereby systematic investigation of the impregnation can be undertaken. Thus one can clarify if the winding or the impregnation of the coil is resulting in weak segments.

The following sections are describing the first experiences and results obtained from the wire qualification experiment.

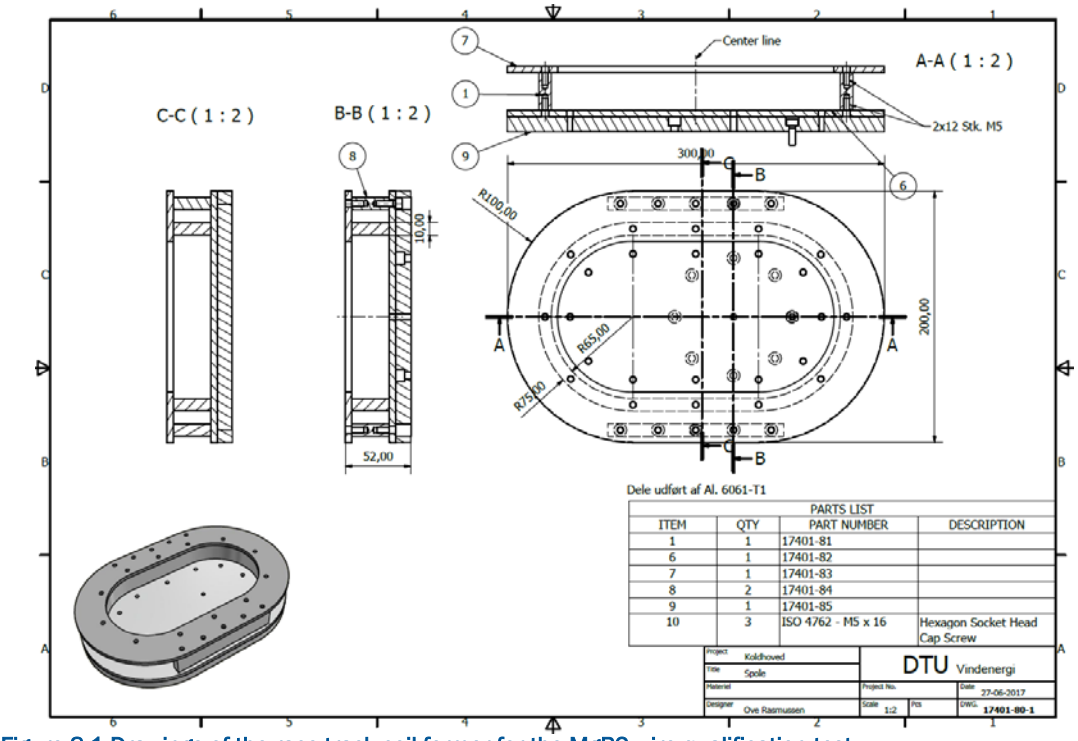

Figure 8-1 Drawings of the race track coil former for the MgB2 wire qualification test.

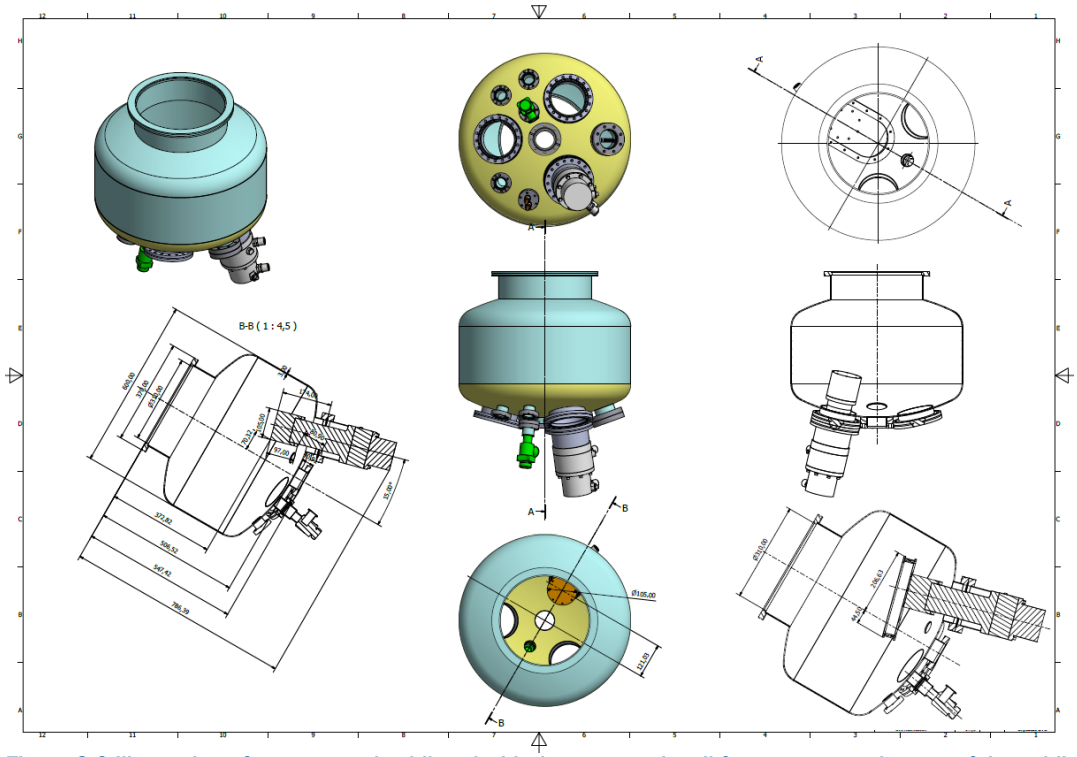

Figure 8-2 Illustration of cryostat and coldhead with the race track coil former mounted ontop of the coldhead on the right hand side. The coldhead is a CH-110 connected to a F-70 helium compressor. The cryostat is mounted in a frame allowing the race track coil former to be inserted through the large flange opening. The coil is connected to current leads going through the cryostat and to an Agilent 6681 power supply. Voltage measurements are done by a Agilent 34420A nano-voltmeter connected to the coil using a separate vacuum feed through also holding the connection to thermometers for measuring the coil temperature.

8.1 First wire qualification coil winding

The first coil winding for the wire qualification test was done using the 1670 wire MgB_2 wire from Columbus Superconductors. A 3 layer winding was done by first winding 3 turns manually at one side of the former and then winding 6 turns side-ways on the coil former (3 x 7 windings in total or about 14 m). Figure 8-3 is showing the 3 layers and Figure 8-4 is showing how the winding was done by extracting the MgB_2 wire from the spool send by Columbus Superconductors and collecting the wire on the coil former mounted in a winding machine. The Winding machine was set to provide a constant small torque to overcome the friction of the spool sliding on the steel rod. There was no attempt to change the torque between winding the end and straight section of the race track, since the force on the wire is seen as very low. The MgB_2 wire was not insulated, since the nickel and copper surrounding the MgB_2 superconductor filaments will appear as insulating if the superconductor turns fully superconducting (with a I_C > 140 A and n ~ 20). The former was insulated using Kapton tape in order not to have any current going into the cryostat.

The current connections to the coil was made using copper braid (4 mm x 0.5 mm) by soldering the copper braid into the MgB_2 copper side. Cable shoes were soldered to the other end of the copper braids in order to connect at a copper bars mounted in the cold plate. 4 twisted wires were soldered to the MgB_2 windings in order to measure the resistance of the MgB_2 wire.

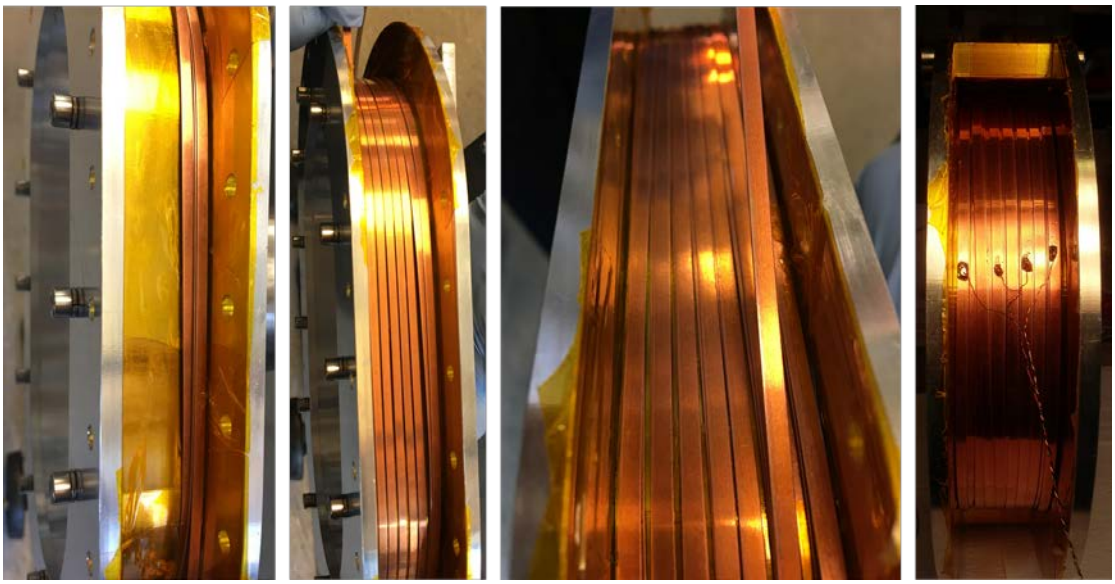

Figure 8-3 Winding of 3 layer coil. From left to right: Winding of 3 turns at side, winding first layer side ways, winding second layer side-ways, final 3 layer with voltage measurement wires soldered to the MgB_2 windings.

Figure 8-4 Manual winding procedure for winding MgB_2 wire onto racetrack coil former. The MgB_2 wire spool is seen in the back and the coil former is mounted onto a winding motor drive in the front. The tension of the wire is provided by the friction of the spool rotating on the steel stick.

8.2 Cooldown

The MgB_2 test coil was mounted in the cryostat shown in Figure 8-2 and covered with Multi Layer Insulation (MLI) in order to minimize the radiation heat load as shown in Figure 8-5. A thermometer was placed on the backside of the cold plate, inside one of the copper blocks for the current leads and also on top of the coil. The voltage wires shown in Figure 8-3 (right) were connected to an Agilent 34420A Nano voltmeter in order to measure the MgB_2 coil resistance. The power supply used for the initial test was an Yokogawa 7651 high precision power supply with the possibility of switching polarity, since only small currents are needed to determine the coil resistance during the cooldown. The thermometers connections were connected to a LakeShore 340 temperature controller in order to convert the sensor resistance to temperature.

The cryostat shown in Figure 8-6 was first evacuated using a turbo pump to a pressure of $P = 10^{-5}$ mbar in about 12 hours. The compressor shown on the right hand side was then turned on, whereby the cold head starts the cooling of the MgB_2 test coil.

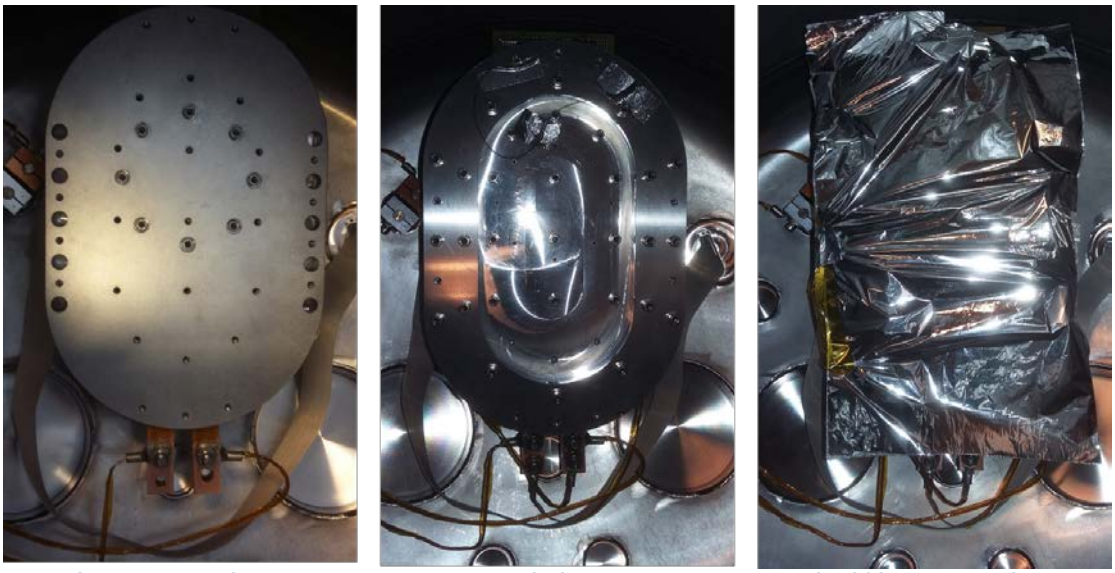

Figure 8-5 Mounting of MgB_2 test coil in cryostat. Left: Cold plate mounted onto CH-110 cold head. Copper bars for the current connections are seen at the bottom and electrical connection for voltage measurements and thermometers are seen to the right. Mid: MgB_2 test coil mounted into the cold plate. Right: Coil wrapped in Multi Layer Insulation (MLI) to reduce radiation heat.

Figure 8-6 Cryostat with turbo pump for establishing the vacuum and electronics for measuring the properties of the superconducting MgB_2 test coil. The cold head sitting in the cryostat is connected to the F-70 helium compressor placed in the room behind the wall (picture to the right).

8.3 Result

The resistance and temperature of the coldplate (cernox) and one of the current cupper block is plotted in Figure 8-7 as function of time during the cooldown performed on 7 October 2017. It is seen that the base temperature of the cold plate and cupper block is reached after about 2 hours of cooling. The MgB_2 coil resistance is decreasing slower than the temperature of the cold plate, indicating that the thermal contact to the cold head is weaker. It should be noted that there is a large difference in the base temperature shown by the cernox sensor indicating a base temperature of about T_{base} ~ 73 K, whereas the platinum1000 sensor sitting in the cupper block is indicating T ~ 40 K. This difference is be believed to be caused by an insufficient thermal anchoring of the cernox sensor to the cold plate, because this was done using aluminium tape. Secondly the rather thick measurement wires connected from the cryostat wall and to the coil are believe to be hard to cool, since they have a large polymer covering as insulation. Finally the Multi

Layer Insulation (MLI) could be placed better on a separate plate in order to be able to provide an intermediate temperature between the coil temperature and the cryostat wall temperature.

A consequence of the base temperature of T ~ 40 K is that the MgB_2 test coil is not getting superconducting. Thus further optimization of the measurement wire connections are needed before the superconducting properties can be measured. Attempts to obtain that will be done before the final INNWIND.EU review meeting.

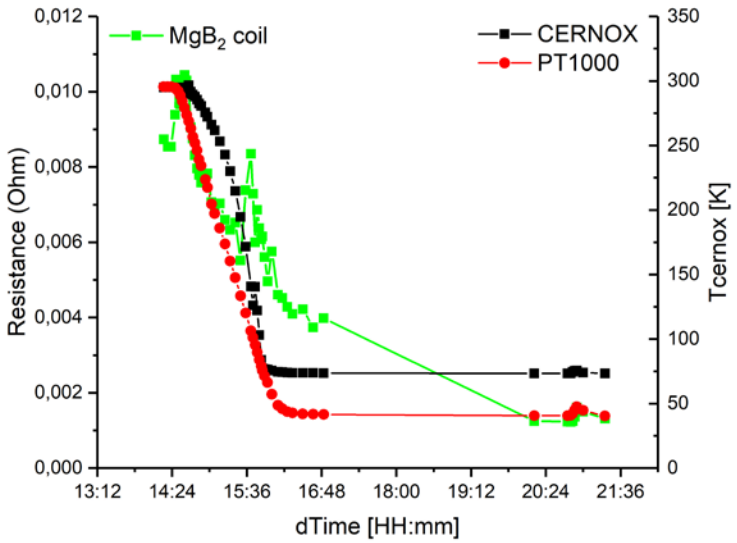

Figure 8-7 Resistance of MgB_2 test coil as function of time on 7 October 2017. The right hand axis is showing the temperature of the cold plate (cernox) and one of the cupper block used for connecting the current leads to the coil. It is seen that a base temperature of the cold plate is reached after about 2 hours of cooling.

8.4 Discussion

Unfortunately the IV curve of the MgB_2 test coil has not yet been obtained for the superconducting state, but a large learning have been obtained from the winding procedure.

The winding machine used for winding the MgB_2 coil has previously been used to a number of race track coils based on high temperature superconducting second generation coated conductor tapes. The previous winding of race track coils used two sources of coated conductors: 1) American Superconductor 344 second generation RBCO tape (Abrahamsen A. , et al., 2011) and 2) Superpower 4050 second generation RCBO tape (Abrahamsen & Jensen, 2012). The coils and the resulting IV curves measured at T = 77 K are shown in Figure 8-8. It can be seen from Figure 8-8 b) that the coil based on the American superconductor resulted in a coil critical current of about 70 A as predicted from the critical current of the tape. Figure 8-8 d) is however revealing that the coil based on the Superpower tape is showing a voltage drop already for currents of about 10-20 A, which is considerable smaller than the critical current of the tape being about 120 A. It was concluded that the tape had been damaged, but it was not possible to determine how (Abrahamsen & Jensen, 2012).

This last curve is however looking strikingly similar to the measurements obtained for the INNWIND.EU MgB_2 race track coil in (Magnusson, Hellesø, Paulsen, Eliassen, & Abrahamsen, 2016). The voltage drop of the INNWIND.EU MgB_2 coil has been analysed in terms of a current sharing model in (Abrahamsen, Liu, & Polinder, 2017) and it was indicated that the weak

segments have a length of 1-5 cm and one coil up to about 36 cm. This analysis has resulted in the formulation of a hypothesis on the origin of the weak segment in INNWIND.EU MgB_2 coil:

1) Potential tape manufacturing process issues were discussed with the director G. Grasso of Columbus Superconductor (Grasso, 2017). It was indicated that the soldering of a copper strip onto the nickel was not as easy as first assumed and the tape used for the INNWIND.EU race track coil has been discontinued at Columbus Superconductors. It was recommended that a wire also used for Magneto Resonant Imaging (MRI) should be considered in the future.
2) Grapping onto the wires with fingers during manual winding might cause local deformation of the MgB_2 wire in a length of about a few cm. Figure 8-3 b) is in the top showing how manual guidance of the wire during the winding of the MgB_2 test coil by using fingers. In the MgB2 test coil wrinkles of the wire resulted.
3) Any manual handling of the wires with fingers during the manufacturing of the wire could result in deformation and creating weak segments.

   It is believed that the MgB_2 test coil can be used to test the above hypothesis and this will be continued after the INNWIND.EU project. Finally the MgB_2 test coil manufacturing is seen as a possible future test method for qualifying MgB_2 wires before winding large coils, but eventually one might consider to test a 1 km spool of MgB_2 by cooling it down and checking if the resistance is vanishing small for small currents.

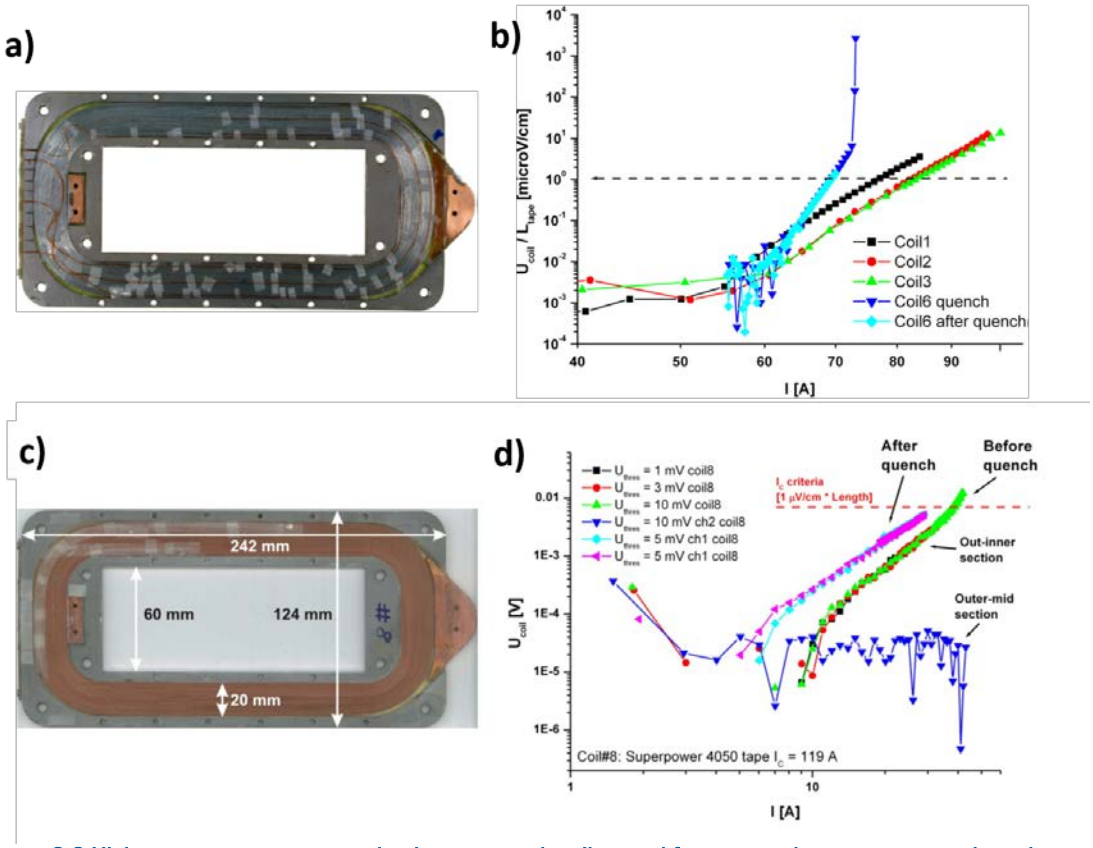

Figure 8-8 High temperature superconducting race track coil wound from second generator coated conductor from American superconductors a) and b) the resulting IV curve measured at T = 77 K (Abrahamsen A. , et al., 2011). The coil in c) was wound from Superpower second generator coated conductor tape and d) the resulting IV curve at T = 77 K (Abrahamsen & Jensen, 2012).

8.5 Conclusion

The winding of the MgB_2 test coil has resulted in the formulation of a hypothesis on the origin of the weak segments observed in the INNWIND.EU race track coil: It might be caused by defect in the wire introducedin the manufacturing or by fingers pressing onto the wire during manual winding. Based on the hypothesis it is recommended that any future attempt to wind large race track coils of MgB_2 wire should be based on fully automatic methods, where no fingers are allowed to touch the wire during the preparation, the winding, soldering onto current leads and the subsequent impregnation. This philosophy was also presented by Theva to have been successfully implemented in the ECOswing project and large coated conductor race track coils are now being produced with no weak segments appearing (Bauer, 2017).